Palacký University Olomouc
Faculty of Science

Department of Optics

Communication over few-mode optical fibers

Diploma Thesis

Nikola Horová

2019

Palacký University Olomouc
Faculty of Science

Department of Optics

Communication over few-mode optical fibers

Diploma Thesis

Author:	Bc. Nikola Horová
Study programme:	N1701 Physics
Field of study:	Optics and Optoelectronics
Form of study:	Full-time
Supervisor:	Mgr. Martina Nováková, Ph.D.
Co-supervisor:	RNDr. Miroslav Ježek, Ph.D.
Thesis submitted on:	.....

Univerzita Palackého v Olomouci
Přírodovědecká fakulta

Katedra optiky

Komunikace v několikamódových optických vláknech

Diplomová práce

Autor:	Bc. Nikola Horová
Studijní program:	N1701 Fyzika
Studijní obor:	Optika a optoelektronika
Forma studia:	Prezenční
Vedoucí:	Mgr. Martina Nováková, Ph.D.
Konzultant:	RNDr. Miroslav Ježek, Ph.D.
Termín odevzdání práce:	.....

Abstract

The aim of this diploma thesis is to investigate the possibilities of transmission of information over telecommunication optical fiber at 800 nm, which is commonly used in free space communication. Telecommunication optical fibers show greater losses and multi-mode behavior at this wavelength. However, sources of non-classical light for quantum communication and single photon detectors have better properties in the field. Part of this work is characterization of telecommunication optical fibers for selected wavelengths in the region 780-1550 nm, measurement of losses dependence on wavelength and time, development of filtration methods of higher modes, and measurements how the state of polarization changes when it is transmitted by fiber in time. Based on the measured data, active correction of fiber communication line instabilities will be designed. The work is a part of the development of the quantum cryptography unified system usable for both - the free-space and the telecommunication fiber communication. The realized fiber telecommunication link should serve to transmit polarization-coded quantum states at 800 nm, while active stabilization can use a strong telecommunication signal.

Keywords

optical fibers, optical telecommunication fiber link, optical losses, modal dispersion in optical fibers, channel fading in optical fibers, polarization

Abstrakt

Cílem práce je prozkoumat možnosti přenosu informace telekomunikačním optickým vláknem na vlnové délce 800 nm, která se běžně využívá při komunikaci volným prostorem. Telekomunikační optická vlákna vykazují na této vlnové délce větší ztráty a vícemódové vedení. Naopak zdroje neklasického světla pro kvantovou komunikaci a jednofotonové detektory mají ve zmíněné oblasti lepší vlastnosti. Součástí práce je charakterizace telekomunikačních optických vláken pro vybrané vlnové délky v oblasti 780-1550 nm, měření ztrát v závislosti na vlnové délce a čase, vývoj metod filtrace vyšších módů a měření změn polarizačního stavu světla přeneseného vláknem v čase. Na základě naměřených dat bude navržena aktivní korekce nestabilit vláknové komunikační linky. Práce je součástí vývoje jednotného systému kvantové kryptografie použitelného jak pro komunikaci atmosférou, tak i telekomunikačním vláknem. Realizovaná vláknová telekomunikační linka by měla sloužit k přenosu polarizačně kódovaných kvantových stavů o vlnové délce 800 nm, zatímco aktivní stabilizace může využívat silný telekomunikační signál.

Klíčová slova

optická vlákna, optická telekomunikační vláknová linka, optické ztráty, módová disperze v optických vláknech, polarizace

Acknowledgment

I would like to thank my supervisor Mgr. Martina Nováková, Ph.D. for her endless patience, advices, for her great support in elaborating my thesis, and for her friendly approach. I am also grateful to her little daughter that she waited for me to finish this thesis with the help of her mom. Another deep gratitude belongs to my co-supervisor RNDr. Miroslav Ježek, PhD. for his very valuable advices. Furthermore, I am also grateful for my both classmates. Thank you for setting up such a friendly environment. Last but not the least, I would like to thank my family and boyfriend for all the care and support.

Declaration

I declare that I elaborated this diploma thesis "Communication over multi-mode optical fibers" independently, under the direction of Mgr. Martina Nováková, Ph.D. and RNDr. Miroslav Ježek, Ph.D. using the resources listed in the references. I agree with the further usage of the thesis according to requirements of Palacký University Olomouc.

In Olomouc..... .....

Contents

1 Introduction and motivation

The thesis deals with a possibility of information transfer at wavelength of 810 nm over telecommunication optical fibers. It is a part of development of the quantum cryptography unified system usable for both - the free space and the fiber communication. The main aim is to build a communication fiber link for two different wavelengths - 810 nm and 1550 nm and progress towards an active correction of its (polarization) instabilities.

The wavelength of 810 nm is commonly used in free-space communication. The main reason is a very good efficiency of silicon detectors at this wavelength. On the other hand, wavelength of 1550 nm is commonly used in the optical fiber communication, because telecommunication fibers show less losses at 1550 nm in comparison with 810 nm. As was mentioned above, the communication fiber link should transfer two beams of light at different wavelengths. The one at 1550 nm should serve to stabilize the link and the second one at 810 nm should transfer information in form of polarization-coded states of individual photons over the fiber link. This could be the way, how to unified free-space and fiber communication. Sources of non-classical light for a quantum communication and single photon detectors have good properties in the area around 810 nm.

The communication over free-space requires direct visibility between transmitter and receiver. The maximum reachable distances in cities are around several kilometers [1] and depend on atmospheric conditions, such as fog, rain, snow etc. In contrast, communication in fibers has now reached a distance over thousands kilometers and is not affected by atmospheric conditions. Even un-regenerated quantum optical links can go as high as 400 km [2]. Furthermore, networks using telecommunication fibers are already built in cities. That incentivizes their use fro quantum communication by plugging convenient sources and receivers . It is true that optical signals at 810 nm has greater losses and shows multi-modal behavior in the telecommunication fiber. The main interest of this work is to see if this problem can be overcome and whether the already built communication networks can be used for the transmission at 810 nm.

Quantum communication at 810 nm using telecommunication fibers has been studied several times over the past few years. Whether it is the system limit operating in the first communication window on a wavelength of about 800 nm, [3], or the transmission of entangled photons at 810 nm over 6 km long network consisting of telecommunication fibers [4]. There was demonstrated high-visibility key distribution over active telecommunication fibers without disruption of classical or quantum signal. Also distribution of polarization entangled photons at 810 nm were measured [5]. Higher-order spatial modes in the telecommunication fiber and their filtering are also discussed here.

The purpose of this work is to analyze an optical fiber link by using different methods of its characterization and find its possible limits. The specific phenomena we were interested in are briefly described in the following paragraphs.

All fibers (the tested communication optical fiber link) used in this thesis to measure the above listed phenomena are Sumitomo 6HFS-S-08210 (fulfill norm G.652 D) and we termed them fiber under test (FUT). FUT may consist of one or fiber pieces terminated

by FC/PC connectors connected together with fiber optical adapters. The available fiber lengths, which can be combined, are 1, 3, 10, 20, and 30 km. If different type of fiber is used, then it is not called FUT.

The transfer over a telecommunication optical fiber is limited for example by losses, dispersion, presence of higher modes, channel fading, and polarization changes. All these phenomena and relevant measurement methods were investigated and each of them is further described in the corresponding section. Each section contains a theory, experimental results, and a discussion of results. This thesis was written in this way mainly for greater clarity.

One of the possible fiber communication limits is determined by the fiber losses. They depend on the fiber length and on the wavelength of the used optical source, which is discussed in the first section. Four various laser diodes were used to determine the dependence of the fiber attenuation on wavelength. During this measurement, we also used different lengths of FUT and their combinations made by optical adapters to measure the fiber attenuation dependence on FUT length.

The next fiber communication limit is given by modal dispersion. The main interest here is the propagation of 810 nm, for which more than one spatial mode is supported in the FUT, because of the larger core diameter of the telecommunication fiber. Temporal delays between the individual modes are larger for longer FUT, which might cause inter-symbol interference. Modal dispersion has the most significant impact on the fiber communication in comparison with all other types of dispersion (if laser diode with narrow spectra are used). The few-mode fiber operation, modal dispersion, and higher-mode filtering are studied in the second section.

The third section contains measuring of channel fading. It is a transmittance dependence on time. Measurement was done to determine the fiber transmittance and how it depends on FUT length. The measurement was also motivated by exploring channel fading in fibers. In free space, this effect is influenced by beam wandering [6], atmospheric conditions, and temperature changes. However, there is no full explanation of channel fading in the fibers and it is still a subject of investigation. Measurements of transmittance changes were made over a long time scale (tens of hours) and they were evaluated by several methods, e.g. by Allan deviation [7] or by using histograms.

Optical time domain reflectometry is discussed in the next section. This method is able to provide information about attenuation in fibers, fiber entire length, position of individual optical adapters in a fiber link, and even about fluctuations or defects in fibers. We used the method for FUT length measurement and to determine the fiber effective refractive index n_{eff}.

Polarization analysis and a possible correction of polarization drifts are discussed in the last two sections. Polarization analysis is very important especially for quantum cryptography, if information is coded into polarization degree of freedom. If we have polarization quantum-key distribution (QKD), our link has to keep the polarization state of light unchanged. Our goal is to determine changes in the polarization state of light, which passed through the FUT and, if there is a change, then suggest a correction that returns the polarization state into the origin one.

2 Optical fiber attenuation

2.1 Attenuation coefficient

When the light signal propagates through a fiber along z-axis, it undergoes attenuation which can be described by the Beer's law [8, 9]

$$\frac{dP(z)}{dz} = -\alpha P(z), \tag{1}$$

where $P(z)$ is the optical power and α denotes the coefficient of attenuation. After solving Eq.(1), we get

$$P(z) = P(0)e^{-\alpha z}, \tag{2}$$

where $P(0)$ is power measured at the input of the fiber and $P(z) = P(L)$ is power measured at the output of the fiber of the length L. The attenuation coefficient can be expressed in units of dB/km by using the relation

$$\alpha = -\frac{10}{L}\,\mathrm{Log}_{10}\frac{P(L)}{P(0)}, \tag{3}$$

where $\frac{P(L)}{P(0)} = T$ is transmission of the fiber.

The α-coefficient is also referred as the fiber-loss parameter. It describes losses of a beam intensity as light passes through a specific material. The larger value of the attenuation coefficient indicates the lower fiber ability to transmit input light. Moreover, the coefficient of attenuation depends on the wavelength of used light $\alpha(\lambda)$ (see Figure 1).

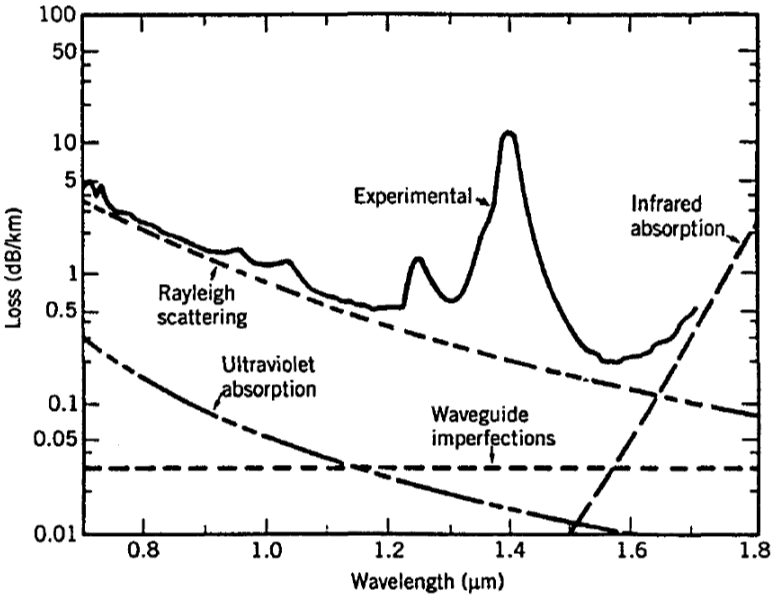

Figure 1: Spectral attenuation of optical silica fibers (solid line). This figure is taken from [9].

2.2 Attenuation coefficient measurement

The attenuation coefficient was measured for different FUT lengths using fiber optical adapters. FUT with lengths of 1, 3, 10, 20, and 30 km specified by manufacturer were used. The experimental values of the attenuation coefficient for particular lengths were obtained by various combinations of these given FUTs. The scheme is in Figure 2.

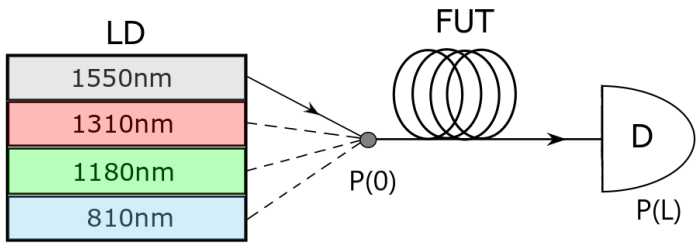

Figure 2: Scheme of the attenuation coefficient measurement. LD- laser diode, FUT- fiber under test, D- detector, $P(0)$ - input power, $P(L)$ - output power.

To varify the losses in the FUT given by manufacturers, this dependence was studied for four laser diodes with different wavelengths. At first, it was necessary to determine the input power $P(0)$ of each diode. This was done using a power meter by averaging of 200 samples, which also determined the standard deviation of obtained values. Afterwards, the final values were corrected for the background radiation.

The individual FUT were combined to various lengths using adapters. They were connected to each diode and the output power $P(z)$ with standard deviation was measured. The final values were again obtained by averaging of 200 samples. Since α depends on factors related with a fiber connection, the measurement of the power attenuation was done four times for each FUT length. Twice with a certain fiber setting and twice when the fiber ends were swapped. Every single adapter had an impact on measured values of the attenuation coefficient. Since every other added adapter meant more radiation losses, we had to consider this fact and make corrections for measured values behind each adapter.

2.2.1 Experimental components description

Four laser diodes with specific wavelengths of 810 nm, 1180 nm, 1310 nm and 1550 nm were used. The range of wavelengths implies that two different power sensors for power meter PM100D made by Thorlabs were needed. Parameters of diodes and power sensors are in Table 1 and Table 2, respectively. Data sheet of the FUT list two values of attenuation coefficient α_0 with respect to two different wavelengths: $\alpha_0 = 0.326$ dB/km for $\lambda = 1310$ nm and $\alpha_0 = 0.185$ dB/km for $\lambda = 1550$ nm.

Table 1: Parameters of used laser diodes

Type	**Made by**	**Serial Number**	λ **[nm]**	**Fiber**	**P(0) [mW]**
QFLD-810-10S	QPHOTONICS	10.12.45	810	SM	10
QFLD-1170-10S	QPHOTONICS	07.16.287	1180	SM	10
FOSS-01-3S-9/125-1310-S-1	Thorlabs	78053-02	1310	SM	1
FOSS-01-3S-9/125-1550-S-1-ISOL	Thorlabs	121524-1	1550	SM	1

Table 2: Parameters of used power sensors

Component	**Type**	**Made by**	**Serial Number**	**Wavelength Range [nm]**	**Power Range**
Standard Si photodiode power sensor	S120C	Thorlabs	13112835	400-1100	50nW-50mW
Slim Ge photodiode power sensor	S132C	Thorlabs	10060822	700-1800	5nW - 5mW

2.3 Results

Transmission T dependence on FUT length L using four various wavelengths of light is shown in Figure 3. As you can see, the negative values of transmission are plotted on the y-axis. The reason is the results processing when output power is normalized by input power and subsequently converted into logarithmic form. The figure shows measured values of transmission for different wavelengths distinguished by colors. Linear regression was used to fit the measured values only of the FUT lengths without adapters [1] and for each wavelength the regression equation was obtained. These regression equations were important for determining the attenuation coefficient α and an influence of the first adapter (connecting FUT with a certain LD) on measured values. Impacts of other two adapters were calculated from an overdetermined system. Correction of each adapter ranges from 1% to 4% and it is shown in Figure 3 by using darker colored markers.

These corrected values are more consistent with the found fit. Models for 1310 nm

[1] Fits were done just for 1, 3, 10, 20, and 30 km long FUT for each wavelength. The measured values of lengths made by connection of fibers by optical adapters are not included in fits.

and 1550 nm are also shown in Figure 3. They are plotted by dashed lines using the values of the attenuation coefficient gained from the FUT data sheet. Measured and corrected values are not too far from the models. Statistical errors are plotted in the figure, too. They are smaller than used symbols. Final values of the attenuation coefficient α for each wavelength λ are listed in Table 3. The letter α_0 represents value of the attenuation coefficient found in the FUT data sheet in case of 1310 nm and 1550 nm. As you can see in Figure 3, the expected value for $\log T$ at $L = 0$ km should be 0, but it is not due to the attenuation caused by the first adapter connecting the FUT with a certain LD. The measured attenuation coefficient α corresponds with the expected dependence [5, 4], which is plotted by solid line in Figure 29 and it is similar to the curve in Figure 1. As you can see, attenuation decreases with increasing wavelength.

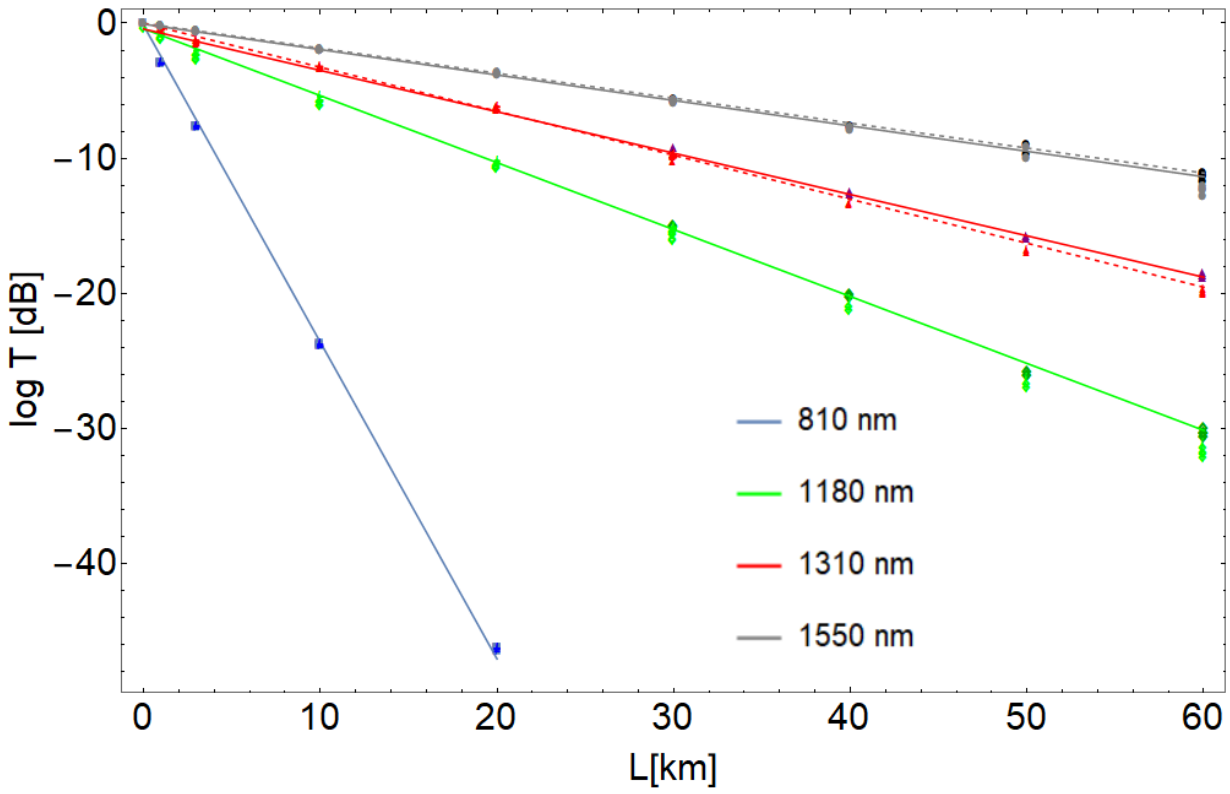

Figure 3: Optical fiber attenuation. Measured values of transmission T for different wavelengths λ are distinguished by colors. Blue, green, red and gray color indicates $\lambda = 810$ nm, $\lambda = 1180$ nm, $\lambda = 1310$ nm $\lambda = 1550$ nm, respectively. Darker colored markers indicate measured data corrected for each used adapter. Dashed lines are models of attenuation for certain wavelengths gained from the FUT data sheet, solid lines are fits of measured data.

Table 3: Measured attenuation coefficient α for certain wavelengths and the corresponding attenuation coefficient α_0 specified in a FUT data sheet.

$\boldsymbol{\lambda}$**[nm]**	$\boldsymbol{\alpha}$**[dB/km]**	$\boldsymbol{\alpha_0}$**[dB/km]**
810	2.35 ± 0.02	-
1180	0.50 ± 0.04	-
1310	0.31 ± 0.05	0.326
1550	0.19 ± 0.04	0.185

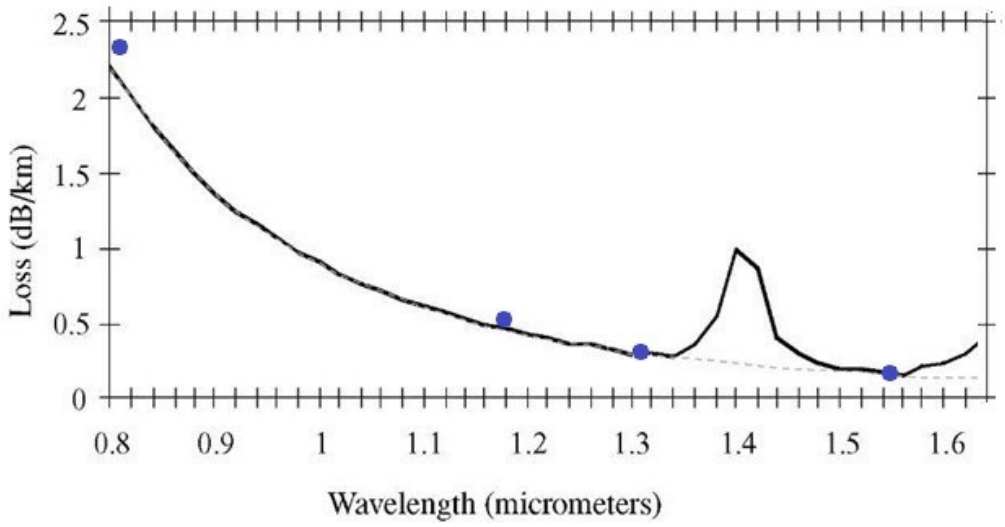

Figure 4: Measured attenuation coefficient α dependence on wavelength plotted by blue spots inserted in graph taken from [10].

Figure 29 shows the dependence of attenuation in fibers α on wavelength λ taken from [10]. Attenuation coefficients for different wavelengths calculated from measured data listed in Table 3 are plotted in this figure by blue spots. The solid line shows total absorption. The peak at $\lambda = 1400$ nm is absorption on OH^- groups. The dashed line shows Rayleigh scattering.

3 Dispersion in fibers, modal dispersion

Attenuation described in the previous section limits the transmission distance by reducing the signal power. However, there are other effects limiting fiber optic transmissions. One of them is dispersion, which limits the fiber bandwidth by broadening optical pulses propagating inside the fiber. Several different types of dispersion may appear in optical fibers: modal, polarization-mode, material, chromatic (waveguide), and nonlinear. The following text will be focused only on the modal dispersion [9].

Modal dispersion occurs in multi-mode fibers due to different group velocities v_g of individual modes. An incident short pulse of light is separated into several individual pulses (modes) while it propagates through the multi-mode fiber of length L. This is schematically shown in Figure 5.

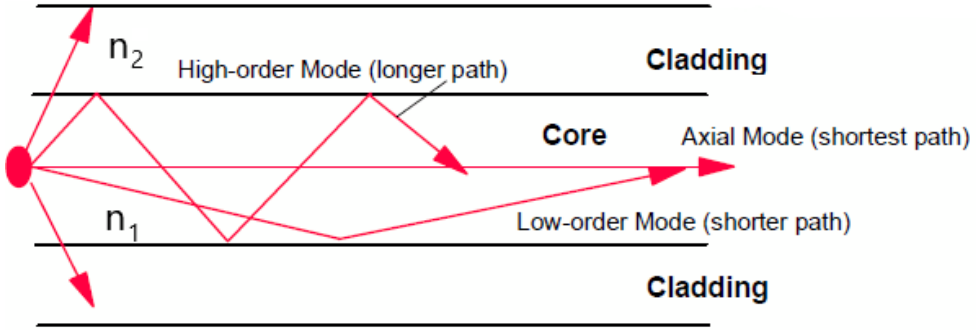

Figure 5: Modal dispersion in a multi-mode fiber. This figure is take from [11] and modified by adding the refractive indices n_1 of a fiber core and n_2 of a fiber cladding.

The number of modes m which can be guided through the multi-mode fiber depends on a wavelength λ, a core radius a, and a numerical aperture N_A defined as the sine of the largest angle accepting and transmitting light through a fiber. These parameters are included in a quantity called normalized frequency V or simply V parameter [8]

$$V = 2\pi \frac{a}{\lambda} N_A. \tag{4}$$

V parameter is closely related with a quantity called normalized propagation constant b defined as [9]

$$b = \frac{n_{eff}^2 - n_2^2}{n_1^2 - n_2^2}, \tag{5}$$

where $n_{eff} = \beta/k_0$ is the effective index, whose value lies in the range $n_1 > n_{eff} > n_2$, n_1 is the refractive index of a fiber core, n_2 the refractive index of a fiber cladding (can be seen in Figure 5), β is a propagation constant, $k_0 = 2\pi/\lambda_0$ is a wavenumber and λ_0 is the input vacuum wavelength. Equation (5) provides two important cases:

- If $b \to 0$ then $n_{eff} \to n_2$. Supported modes are poorly guided inside a fiber.
- If $b \to 1$ then $n_{eff} \to n_1$. Supported modes are well guided inside a fiber.

Relation between V parameter and propagation constant b for a step-index fiber is shown in Figure 6 (a). It shows b for a number of linear polarized (LP) modes as a function of V, where LP_{01} is the basic spatial mode. We can see that a fiber with a large value of V supports many modes [8, 12].

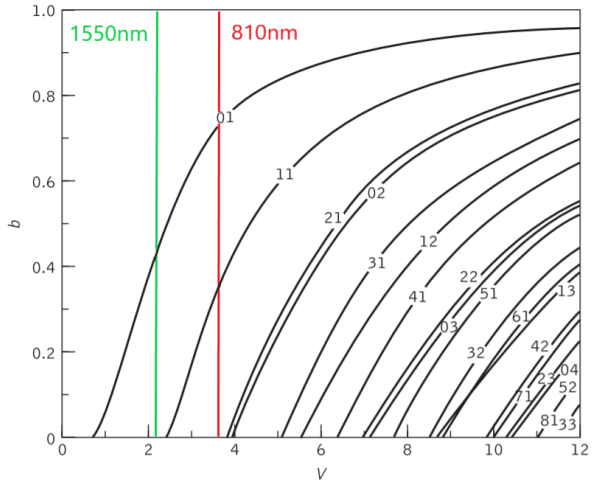

(a) Normalized propagation constant b as a function of normalized frequency V. This figure is taken from [12] and modified of the curve referring to calculated V parameter of our FUT at 1550 nm and 810 nm.

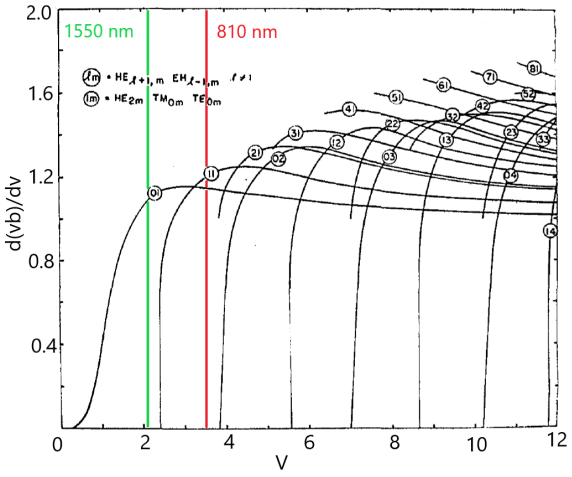

(b) Normalized group delay d(Vb)/dV as a function of normalized frequency V. This figure is taken from [13] and modified of the curve referring to calculated V parameter of our FUT at 1550 nm and 810 nm.

Figure 6: (a) and (b) describing phase and group velocity of individual excited modes in the FUT, respectively.

Figure 6 (a) refers to the phase velocity of individual modes. However, we are mainly interested in energy transfer and it is associated with the group velocity of modes depicted in Figure 6(b). In figures, we can see that higher modes have greater phase velocity than group velocity. This is mainly due to the fact that the higher modes have larger MFD (mode field diameter), which more extends into the fiber cladding. The fiber cladding has a smaller refractive index than a fiber core. Therefore the modes can better propagate there. In Figure 6, a curve for the V parameter corresponding to the number of LP modes supported in the FUT is plotted. V parameter is calculated from Equation (4) and from given parameters of the FUT in its data sheet. In case of 1550 nm, $V \approx 2.1$ and only one mode is supported, because if $V < 2.405$, then fiber supports only one mode and if $V \geq 2.405$, then the fiber supports more than one mode [8]. In case of 810 nm, $V \approx 3.6$, due to it the FUT supports two modes.

We now assume that a fiber of length L have a large value of V parameter, so the other modes m are also present in the fiber. Several LP modes, which can be excited in step-index fiber are plotted in Figure 7. Modal dispersion then causes separation of these pulses, which increases with increasing L. As was mentioned above, separation appears

due to different group velocities v_g of individual modes.

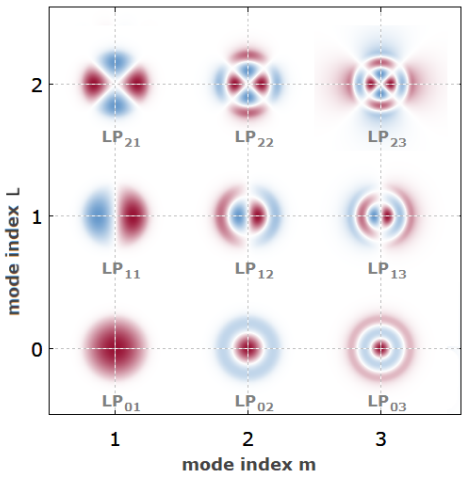

Figure 7: Electric field amplitude profiles for several guided modes LP_{lm} of a step-index fiber. l corresponds to the number of intensity peaks in the radial direction and $2m$ corresponds to the number of intensity peaks over 360 degrees in the azimuthal direction. This figure is taken from [14] and subsequently cropped to only a few LP modes.

3.1 Phase and group velocity

Phase velocity v_p is the velocity of points propagating with a constant phase in a wave. If the wave propagates along a fiber in z direction, phase velocity is given by [12]

$$v_p = \frac{\omega}{\beta}, \tag{6}$$

where ω is the angular frequency of the wave and β is the propagation constant.

Let us now consider a group of waves with closely similar frequencies instead of one wave. Their combination forms a wave packet. We no longer see that the packet propagates at the phase velocity of individual waves but it moves at a group velocity v_g defined as [12]

$$v_g = \frac{\delta\omega}{\delta\beta}. \tag{7}$$

Higher order modes, whose propagation directions have the greater angles with the fiber axis, have the lower propagation constant β. Different modes therefore have different group velocities. Mode propagating at the greater angle with the fiber axis has lower group velocity. As a result of longer distances between individual reflections, this mode is more delayed. This can also be seen in Figure 5 [9].

3.2 Modal filtering

If we need to work only with a basic mode in the multi-mode fiber, it is necessary to filter higher-order modes. There are several ways to do it [15]:

- Winding a certain length of a fiber on a reel with a small diameter. The longer the fiber length is wound, the better the higher modes are filtered. We can also reach the same effect by using smaller diameter.

- Using a single mode fiber behind a multi-mode fiber.

- Spatial filtering of the light at the output of the multi-mode fiber.

The first two items are measured and discussed below.

3.3 Modal dispersion measurement

The use of the wavelength $\lambda = 810$ nm implies that our the FUT becomes a multi-mode fiber. We have to determine, how many modes we are able to measure and how we can filtered them out. The experiment is shown in Figure 8. Here the short optical pulses propagate from SMF 780-HP to the FUT. The output optical signal is analyzed by a fast detector and oscilloscope, where the time separation of detected modes is observable.

3.3.1 Experiment and its components description

The work with individual optical pulses was achieved by using homemade pulser, an electric device, which needs power supply of ±9 V from the source TTI PL303QMD (quad mode dual power supply, SN: 444528). The pulser drove the laser diode QFBGLD-808-5 by QPhotonics with the current threshold $I_{th} = 17$ mA, the operating rate $I_{op} = 34$ mA and the central wavelength $\lambda = 808.3$ nm. The laser diode was below its threshold. The reason is that the diode had not been emitting continuously but the individual pulses still had to be detected. Then optical pulses passed through the SM 780-HP fiber to our FUT. The optical signal from the FUT output went into a detector DET025AFC/M by Thorlabs. After that, the electric signal was amplified by ZX60-P103LN+ an inverting amplifier (SN: SF716801706) Mini-Circuits with power supply of 5V. And finally the amplified converted electric signal was processed by the oscilloscope LeCroy WAVEPRO 7Zi (bandwidth 1.5GHz - 6 GHz).

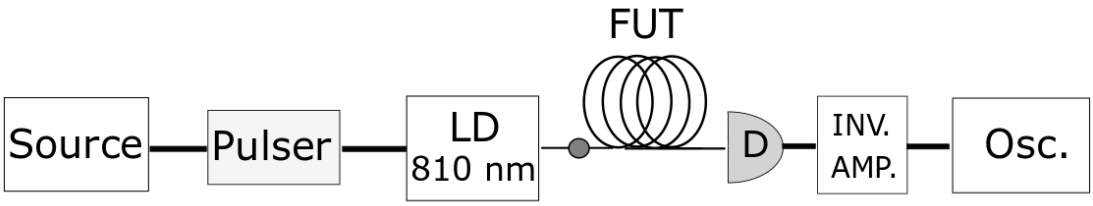

Figure 8: Optical setup for modal dispersion measurement. LD - laser diode, D - detector, INV. AMP. - inverting amplifier, Osc. - oscilloscope, and small gray round point - optical adapter.

The mode dispersion measurement was done for various lengths of the FUT. Two peaks belonging to LP_{01} and LP_{11} were observed. Individual peaks of measured data corresponding to individual modes were subsequently fitted by parabola functions and by using their regression equations the extremal values of each peak were counted. Then the coordinates of extremal points on x-axis (time axis) were determined. These values were subsequently subtracted for each measurement of modal dispersion to find a delay τ between two individual modes.

3.4 Results

As was already mentioned, the FUT becomes the multi-mode fiber for a certain wavelength λ. Supported modes in the FUT have increasing time delays to each other with an increasing length of the FUT L. This conclusion is listed in Table 4. We can see that the time delay τ is a linear function of L. The average delay (per one kilometer) is $\tau_{1\mathrm{km}} = (2.1 \pm 0.2)$ ns. The error is counted from average of all errors from all measurement of modal dispersion per one km containing the statistical error. The same result is for example in [5, 4], where the average value of delay is $\tau = (2.2 \pm 0.2)$ ns. As we can see from the calculated values of delay τ_{1km} listed in Table 4, whenever the combination formed with 1 km long FUT was measured, we got higher values of τ_{1km} than in other cases. This is probably due to the fact that this FUT is slightly longer than was stated.

Table 4: Modal dispersion measurement. L is the length of the FUT, τ is the time delay between individual modes and $\tau_{1\mathrm{km}}$ is the time delay per 1 km of FUT length.

L[km]	$\boldsymbol{\tau}$**[ns]**	$\boldsymbol{\tau_{1\mathrm{km}}}$**[ns]**
3	6.01 ± 0.15	2.00 ± 0.02
4	8.59 ± 0.13	2.58 ± 0.01
10	20.83 ± 0.13	2.04 ± 0.01
11	23.13 ± 0.18	2.30 ± 0.02
13	26.87 ± 0.23	1.87 ± 0.02
14	28.91 ± 0.20	2.05 ± 0.02

For our purpose we need to operate only with the basic mode LP_{01}. Thus we tried to filtered out the higher modes by several methods. The first: The higher modes were filtered by winding an ending length of the FUT on a reel with a diameter $d \approx 0.5$ cm. The result is shown in Figure 9. There we have 10 km long FUT, where the mode dispersion is easily observable. We can see, that by subsequent winding of the FUT on a reel the mode represented by the second peak is disappearing, while the amplitude of the basic mode represented by the first peak is not influenced (two modes LP_{01} and LP_{11} are measured). The second method was based on a 30 cm long single-mode fiber situated

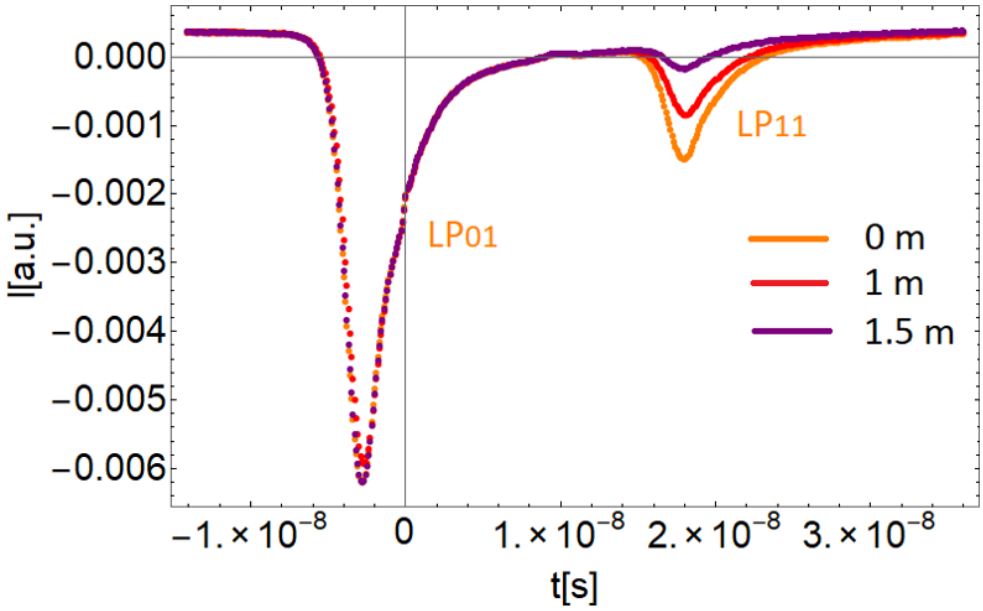

Figure 9: Modal filtering of the 10 km long fiber. We see the gradual fading of the second peak belonging to the higher-order mode. Orange colored markers indicate a state without filtering. Red markers show a case when 1 m of total fiber length is coiled on a reel with diameter $d \approx 0.5$ cm. Purple markers represent the case when the winding length is 1.5 m.

behind the FUT. The mode was also filtered out. On the other hand, both methods had a big disadvantage. The wavelength $\lambda = 1550$ nm is not anymore guided by the FUT. In the first case, the reason is that $\lambda = 1550$ nm needs a smaller diameter to be radiated out than $\lambda = 810$ nm. In the second case, the short single mode fiber probably contains elements absorbing $\lambda = 1550$ nm.

In the end, we used a 6.5 cm long single-mode fiber connected to the FUT. This fiber transmits the wavelength of 810 nm and the transmittance for 1550 nm is around 50%.

4 Channel fading

Any transmission of information by air or by fiber is sensitive to transmittance fluctuations caused by atmospheric turbulence or temperature changes. This phenomenon is called channel fading. It is more observable in free-space communication, where the impact of air turbulence and temperature changes are more radical. On the other hand, it is also observable during communication over a fiber in long time scales. However, this phenomenon has not been too much explored so far.

4.1 Measurement of channel fading in fibers

Influence of channel fading was investigated mainly for LD QFLD-810-10S-SM ($\lambda = 810$ nm, maximal operating current $I = 87$ mA) by QPhotonics. The signal from the LD was split in two halves by a beam splitter 50:50 (SIFAM 01199313). The first half went into the FUT and then through the SMF 780-HP to the detector PDA36A-EC (wavelength range: 350 - 1100 nm). The second half went directly in the detector of the same type as the previous one and it was taken as reference. Both detectors were connected to ADC (analog-to-digital converter), through which the long-term measurements were set. The sampling rate was 3 samples per second. This ADC needed power of 12 V, so it was powered by source TTI PL303QMD (quad mode dual power supply (SN: 444528) with a voltage range of 0V-30V and current range of 0A-3A). The channel fading effect had been measured for 62 hours (almost 3 days). The scheme of this experiment is depicted in Figure 10.

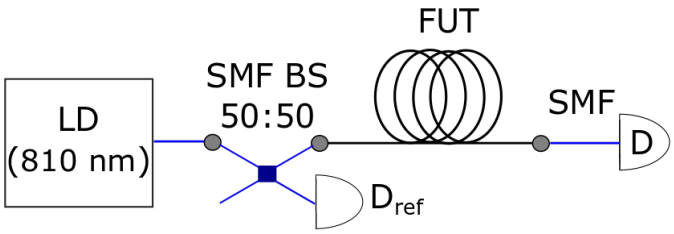

Figure 10: Setup of the channel fading measurement. Blue lines indicate a single mode fiber (SMF), LD - laser diode, D - detector.

4.2 Results

Fluctuations in transmittance were measured for several configurations: no FUT, 1 km, 4 km, and 10 km long FUT each for 62 hours. The length of 4 km was made by connection of 1 km with 3 km long FUT. At first, the measurement was done without FUT situated in one arm of BS 50:50. One output of BS 50:50, let's call it signal arm, was connected to SMF 780-HP and then with detector, the second one, reference arm, was directly connected with the detector. The signal at both detectors was 10 dB amplified. The measured data

from the detector placed in signal arm were divided by the data from detector in reference arm and normalized to 1 according to maxima. The result is plotted in Figure 11(a).

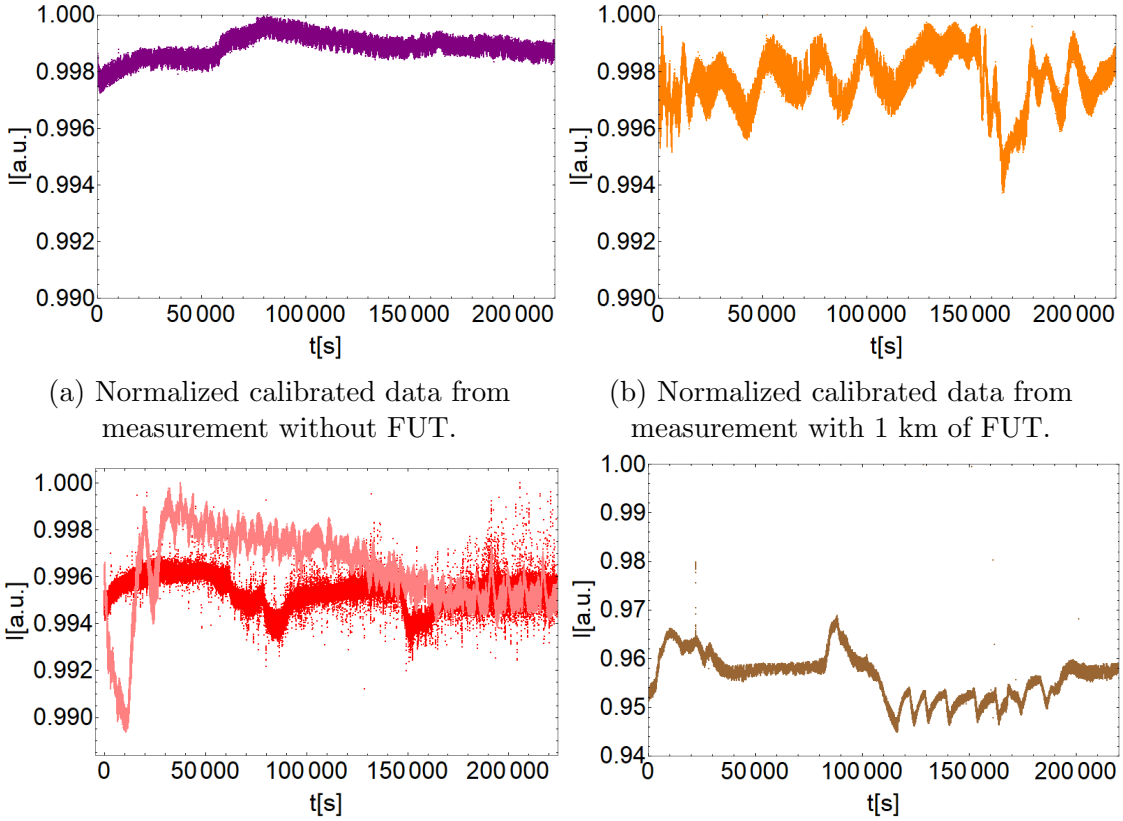

(a) Normalized calibrated data from measurement without FUT.

(b) Normalized calibrated data from measurement with 1 km of FUT.

(c) Normalized calibrated data from the measurement with 4 km of FUT.

(d) Normalized calibrated data from measurement with 10 km of FUT.

Figure 11: Relative intensity measured during 62 hours.

Then we left the same connection as was in the first case, only 1 km FUT was placed in signal arm and connected to the SMF. Whole process of measurement was repeated. We also 10 dB amplified the signal from both arms of BS 50:50. The measured data were processed in the same way as data in the first case and they are plotted in Figure 11(b).

After that, 3km long fiber was connected with 1 km long one in signal arm of BS 50:50 to create 4 km long FUT. Whole process of measurement was repeated, but in this time we 30 dB amplified the signal in signal arm of BS 50:50, while reference arm had still 10 dB amplified signal to utilize whole range of ADC. The result of measured data, which were processed in the same way, is plotted in Figure 11(c). This measurement was repeated to see, if the measurement is repeatable under laboratory conditions.

Finally, the same measurement was done for the case of 10 km long FUT and the whole process of measurement was repeated again. The output signal from signal arm of BS 50:50 with 10 km long FUT was 40 dB amplified, while reference arm was still 10 dB amplified. Gained data were processed in the same way and they are plotted in Figure 11(d).

To determine the impact of laboratory conditions on the fiber transmittance, the Allan deviations δA of all measured data for different lengths of the FUT were calculated by [7]

$$\delta A = \sqrt{\frac{1}{2(n-1)} \sum_{i=0}^{n} [y(\tau)_{i+1} - y(\tau)_i]^2}, \tag{8}$$

where n is the number of time bins of length τ and y_i is the average value of intensity in each time bin. The sampling of ADC determined the lowest value of τ and the total time of measurement determined the highest value of τ.

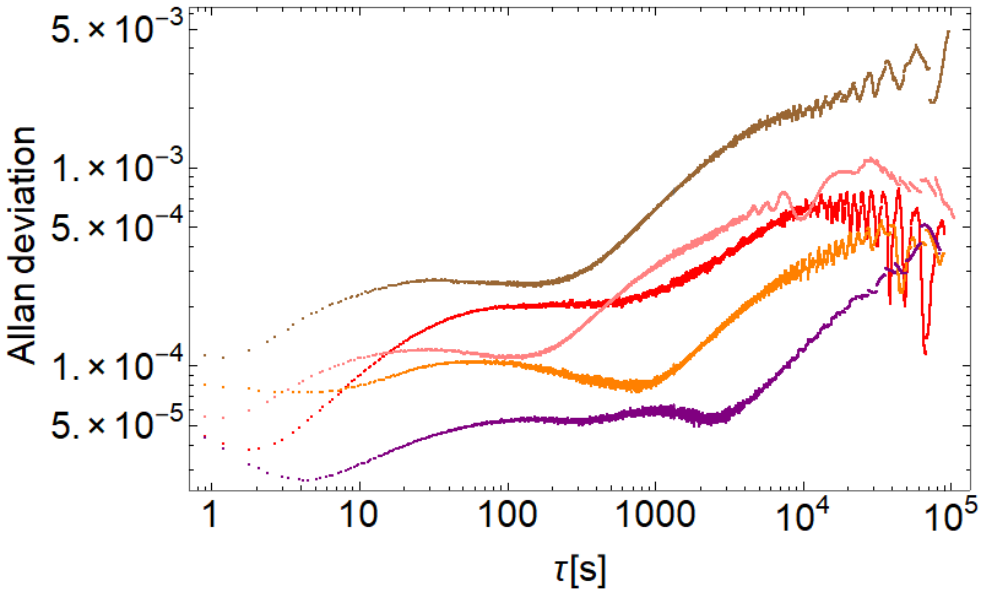

Figure 12: Allan deviation calculated from the data plotted in Figure 11 describing the fluctuations in transmittance caused by conditions in a laboratory. Brown color indicates the case of 10 km long FUT put in signal arm of BS 50:50. Red and pink colors indicate the case of 4 km long FUT, by orange color is plotted the case of 1 km long and the case with no FUT is plotted by purple color.

Measured data processed by Allan deviation (8) are plotted in Figure 12. The case of no FUT is plotted by purple color, 1km long FUT by orange color, 4 km long FUT by red and pink color and 10 km long FUT by brown color. The trend of the Allan deviation curve starts at higher values due to noise. With increasing τ, the Allan deviation decreases because the noise averages out. Then it starts increasing due to fluctuations caused by temperature changes or other conditions in the laboratory.

In Figure 12, the described trend of our curves is observable. However, at the integration time of 34 hours, the Allan deviation is about 0.008% in case of 1 km and 0.05% in case of 10 km long FUT. With an increasing length of FUT, the fluctuations in transmittance also increases. For large values of τ, there are "oscillations" caused by sampling errors. To

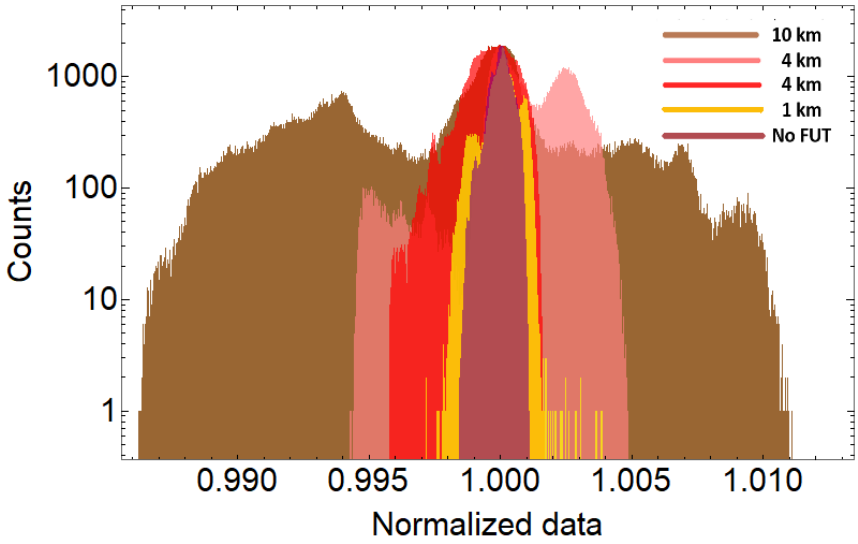

Figure 13: Histograms of normalized data according to their statistical mode (most common value) and according to the same height.

reach a higher precision and more pronounced drifts, we need to do longer measurement (lasting about few weeks).

We have also plotted transmittance histograms for various FUT lengths to show a distribution of transmittance fluctuations, see Figure 13. The histograms are normalized according to their statistical mode (most common value) and according to the same height. Purple color refers to measurement without FUT, by orange color is plotted histogram for 1 km long FUT, pink and red belongs to histograms of 4 km long FUT, and by brown color is plotted histogram of 10 km long FUT. Histogram of measurement without FUT shows the accuracy of measuring devices and we can see from other histograms that other measurements are not limited by this accuracy. For transmittance fluctuations, we expected a pattern similar to that for 4 km, which is plotted by red color in Figure 13. However, we got variously shaped histograms of our measured data. Unfortunately, the measurements were not performed under the same conditions, so even if we measured the 4 km long FUT twice, we cannot assure anything about the repeatability of the measurements. The laboratory conditions may be the cause of such various histograms, or not sufficient time of acquisition.

5 Optical time domain reflectometry (OTDR)

OTDR device serves for an optical fiber (link) analysis. Its function is based on Rayleigh scattering and back reflection of input light. It can provide information about attenuation in fibers, their entire lengths, position of individual optical adapters in a fiber link and even about fluctuations or defects in fibers [12].

Fiber link, FUT, is connected to OTDR device just by one end. The OTDR device sends a pulse of light into the FUT, subsequently analyses the optical signal, which comes back, and measures the travel time. A part of the pulse is scattered on small fiber particles in all directions. Some is scattered back into the device. This effect of Rayleigh's backscattering is present in the entire length of the fiber, so we can gain information about the real fiber length. Information about optical adapters, defects etc. are gained from Fresnel reflection caused by different density of the used material [12, 16].

Fresnel's reflection always occurs when light passing through the optical fiber encounters a different density material. Then a small amount of light (about 4%) is reflected back and the rest of it passes in the original direction. Different densities are mainly at the fiber end and at the adapters connecting two fibers. If larger Fresnel reflection goes back towards the source, dead zones can occur. It happens because the OTDR device measures only a small amount of back-reflected and backscattered light. In case of high reflection, the sensor becomes saturated and it is unable to measure lower reflections and backscattered light [16].

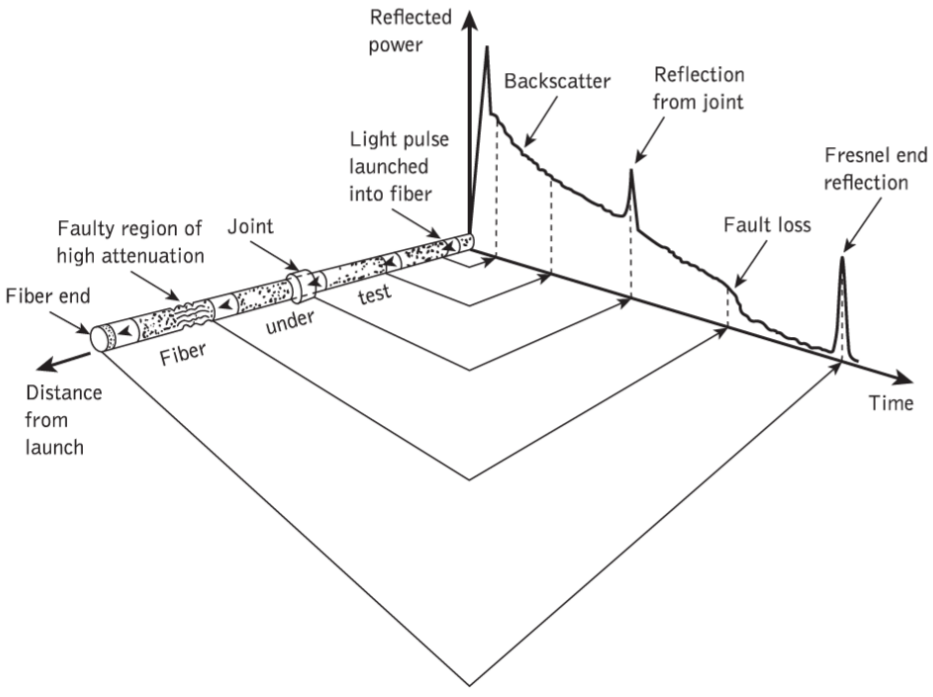

Figure 14: An illustration of OTDR output using FUT. This figure is taken from [12].

The example of output of the OTDR device is plotted in Figure 14. It shows the reflected power dependence on time. We can see backscattering, defects, and two cases of reflection: from a joint (optical adapter) and from the fiber end.

5.1 OTDR measurement

The OTDR device was used to determine the real length of the FUT and to determine the effective refractive index for different FUT lengths (1 km and 3 km). The schema of our measurement using OTDR method is plotted in Figure 15. Pulse generator TTi TGP110 10MHz created 1 ns positive electric pulses, which were inverted (the negative pulses were created) to drive the LD (QFLD-808-50S-PM (SN: 12.12.805, PM fiber coupled, 808 nm, 50 mW by QPhotonics). Optical pulses from LD went into the fiber circulator (FOC-12P-111-5/125-SSS-810-50-3A3A3A-1-1 by OZ Optics). The circulator is three-port optical device, let's name the ports 1, 2, 3. When light comes from port 1, it exits port 2, where the FUT is situated. However, when a part of light passing through port 2 is reflected back, it does not come back to port 1 but it exits port 3. Light in port 3 went into the detector DET025AFC/M by Thorlabs and inverting amplifier ZX60-P103LN+ (50-3000 MHz). Then the signal was processed by oscilloscope LeCroy WAVEPRO 7Zi (bandwidth 1.5 GHz - 6GHz).

Used fibers are SMF 780-HP with different lengths $l_{1g} = 2.056$ m and $l_{2g} = 2.998$ m.

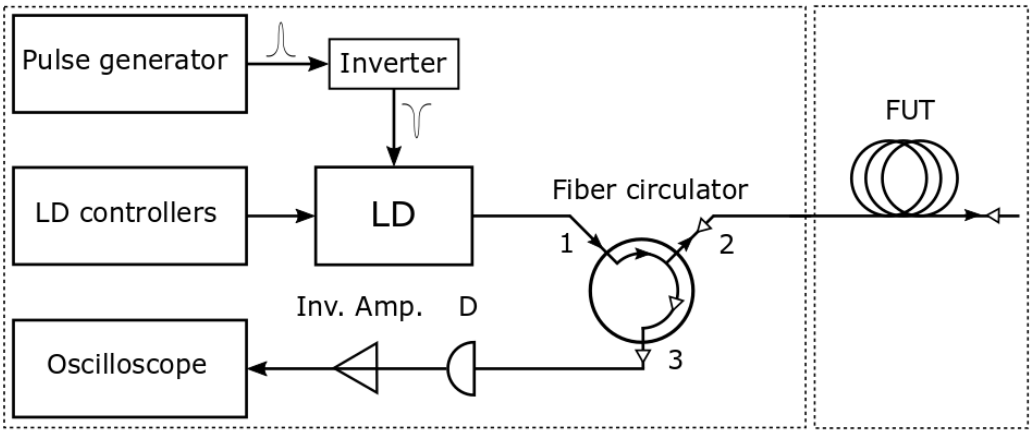

Figure 15: Schema of OTDR measurement. LD - laser diode, Inv. Amp. - inverting amplifier, D - detector.

5.1.1 OTDR device used to verify fibers length

The OTDR device was used to verify the length of the used SMF. It was done in two ways:

- Knowing the length l_2 of the SMF connected with the SMF of the "unknown" length l_1. The measurement must satisfy the assumption that both used fibers are

of the same type, i.e. $n_{\text{eff1}} = n_{\text{eff2}} = n_{\text{neff}}$. In this case we can determine l_1 from the equation

$$l_1 = \frac{\Delta t_1}{\Delta t_2} l_2, \tag{9}$$

where Δt_1 is the measured delay between the first and the second peak of measured data. The first peak was created by reflection on the adapter connecting the fiber of port 2 of the fiber circulator with the fiber of length l_1. The second peak was created by reflection on the adapter connecting the fiber of length l_1 to the fiber of length l_2. Δt_2 is the measured delay between the second and the third peak of measured data. The third peak was created by the reflection on the end of the fiber of length l_2. This measured data are plotted in Figure 16.

- Knowing effective refractive index n_{eff} of the SMF. In this case we can determine l_1 from the equation

$$l_1 = \frac{c}{2n_{\text{eff}}} \Delta t_1, \tag{10}$$

where c is the light velocity, n_{eff} is the effective refractive index of the fiber with "unknown" length l_1 and Δt_1 is the measured delay described above.

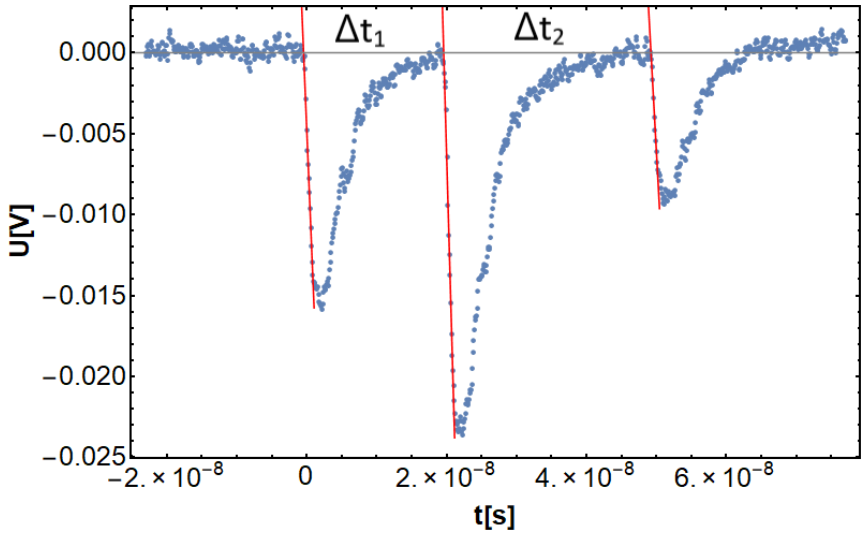

Figure 16: Measured delay between reflected pulses at adapters and at the end of the last fiber. Blue dots are measured data, the red curves are linear fits.

The individual delays of both fibers were found from measured data using linear fit of pulse leading-edges. Then the intersections of x-axis (time axis) with these fitted curves of pulse leading-edges were found. Finally, the first intersection with the second and the second intersection with the third were subtracted to determine delays Δt_1 and Δt_2 between individual pulses.

The first way to calculate the fiber length was to determine the delays Δt_1 and Δt_2 between individual pulses and to determine fiber length l_1. The delays determined from

the measured data were $\Delta t_1 = (2.00 \pm 0.08) \cdot 10^{-8}$ s and $\Delta t_2 = (2.96 \pm 0.05) \cdot 10^{-8}$ s. The "unknown" fiber length $l_1 = (2.03 \pm 0.01)$ m was calculated using Equation (9) and from knowledge of $l_2 = 2.998$ m. As we can see, our value of l_1 varies by about 1.4% from the given length $l_{1g} = 2.056$ m.

The second way to calculate the fiber length was derived from the knowledge of the effective refractive index $n_{\text{eff}} = 1.48$, which belongs to the fiber of "unknown" length l_1 and by using Equation (10). The calculated value is $l_1 = (2.03 \pm 0.01)$ m.

These results are mainly influenced by the uncertainity of determining the delays between the individual pulses. All errors are statistical and they are determined by the curve fits.

5.1.2 Determination of the fiber effective refractive index using OTDR

In this part is described how to determine the effective refractive index of our 1 km and 2 km long FUT. At first, SMF was changed by 1 km long FUT in port 2 of the fiber circulator. Then the measurement was exactly the same as in the previous experiment: The optic pulses were sent from port 1 into port 2, where the FUT was situated. Then the reflected pulses from port 2 went into port 3, where they were analyzed. The results are plotted in Figure 17.

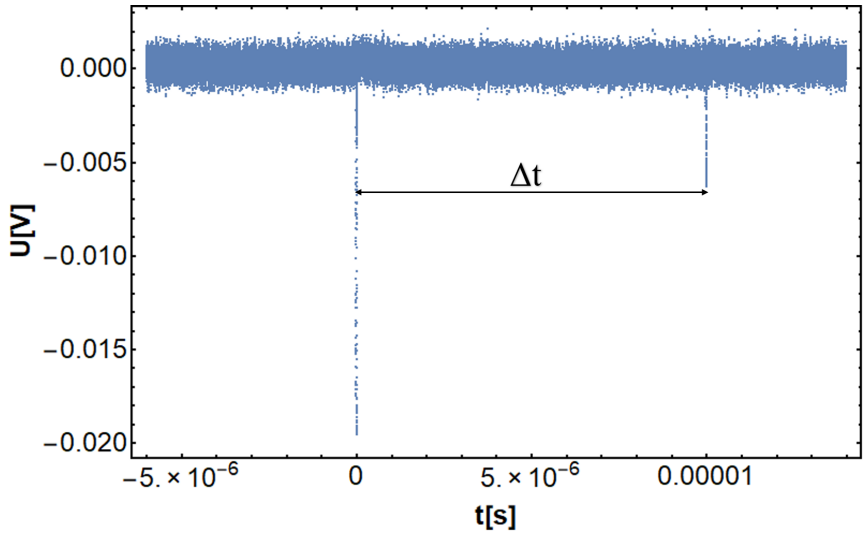

Figure 17: Measured OTDR data of 1 km long FUT. We can see two reflections; the first one is the reflection at the adapter connecting FUT and port 2 of the fiber circulator and the second reflection is at the end of 1 km long FUT.

There were two reflections: one at the adapter connecting FUT with port 2 of the fiber circulator and one at the end of FUT. By fitting the leading-edges of the individual peaks in measured data and by determining the intersections of these fitted curves with the time axis, we could find the delay between the first and the second peak. Then we calculated

the effective refractive index n_{eff} of this FUT by

$$n_{\text{eff}} = \frac{c\Delta t}{2L}, \tag{11}$$

where c is the light velocity and L is the length of the FUT.

The same process of the measurement was done for 3 km long FUT. The result is plotted in Figure 18.

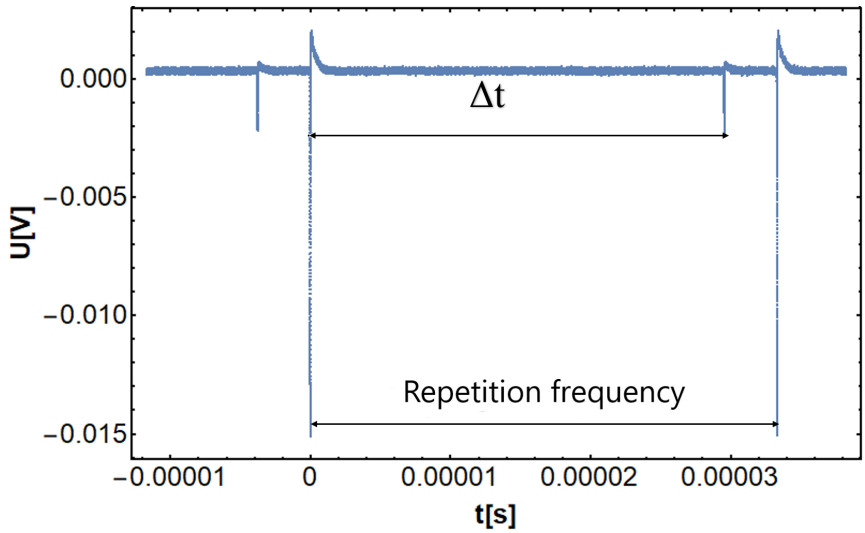

Figure 18: Measured OTDR data of 3 km long FUT. We can see two reflections; the first one is the reflection at the adapter connecting the FUT and port 2 of the fiber circulator and the second reflection is at the end of 3 km long FUT.

The value of the effective refractive index of 1 km and 3 km long FUT was calculated from the Equation (11) and from the knowledge of the FUT length. In case of 1 km long FUT, the delay between individual pulses was $\Delta t_{1km} = (2.96 \pm 0.06) \cdot 10^{-5}$ s and the effective refractive index was $n_{\text{eff1}} = 1.48 \pm 0.03$. In case of 3 km long FUT, the delay between individual pulses was $\Delta t_{3km} = (9.99 \pm 0.08) \cdot 10^{-6}$ s and the effective refractive index was $n_{\text{eff3}} = 1.50 \pm 0.01$.

6 Polarization analysis

6.1 Polarization

Light is an electromagnetic wave described by its electric field vector. When the beam of light propagates through a medium, this vector oscillates in time and space. Considering only a transverse wave in an isotropic medium, there are only two independent directions of electric field vector oscillations of such a wave. The most general case of polarization is elliptic polarization. The beam of light is said to be elliptically polarized if the end of the electric filed vector traces an ellipse in the xy plane. Linearly and circularly polarized states are the special cases of the elliptically polarized states [17].

The electric field vector $\vec{E}(\vec{r}, t)$ can be written

$$\vec{E} = \vec{A} \exp{(\omega t - \vec{k} \cdot \vec{r})}, \tag{12}$$

where ω is the angular frequency, t propagation time, $\vec{k}$ is the wavevector, $\vec{r}$ is the position vector, and $\vec{A}$ is the amplitude (constant vector). The term in brackets is usually known as the phase $\Delta = \omega t - \vec{k} \cdot \vec{r} + \delta_0$, where initial phase $\delta_0 = 0$. Only the real part of the right side of the equation represents the actual electric field.

If we consider only the propagation in the z-axis, the electric filed vector lies in the xy plane and we can write two independent equations for its two independent components z, t

$$\begin{aligned} E_x &= A_x \cos{(\omega t - kz + \delta_x)}, \\ E_y &= A_y \cos{(\omega t - ky + \delta_y)}, \end{aligned} \tag{13}$$

where amplitudes A_x and A_y are positive and independent and δ_x, δ_y are two independent initial phases describing the relation between two components of the electric field vector. From the definition $\delta = \delta_y - \delta_x$, where $-\pi < \delta \leq \pi$ [17].

Now we can define the linear and circular polarization using defined independent phases δ_x and δ_y. For simplicity, we will not consider periodicity of cosinus function

- If $\delta = \delta_y - \delta_x = 0$ or π, the electric field vector oscillates in a constant direction and the light beam is said to be linearly polarized. When $\delta = 0$, then two components of oscillation are in phase and when $\delta = \pi$, then these components are out of phase [17, 18].
- If $\delta = \delta_y - \delta_x = \pm\pi/2$, the electric field undergoes uniform rotation in the xy plane and the light beam is said to be circularly polarized. The beam of light can be right-handed or left-handed polarized. It depends on convention. In our case $+\pi/2$ is right-handed and $-\pi/2$ left-handed polarized beam of light [17, 18].

The equation of the ellipse can be found by eliminating ωt at $z = 0$ in Equation (13). We obtain

$$\left(\frac{E_x}{A_x}\right)^2 + \left(\frac{E_y}{A_y}\right)^2 - 2\frac{\cos\delta}{A_x A_y} E_x E_y = \sin^2\delta. \tag{14}$$

6.2 Stokes parameters, Jones calculus, and Poincaré sphere

Polarization states of light can be described by a set of parameters called Stokes parameters S_0, S_1, S_2 and S_3. They are measurable quantities defined as [18]

- $S_0 = \langle A_x^2 \rangle + \langle A_y^2 \rangle$ is total flux density.
- $S_1 = \langle A_x^2 \rangle - \langle A_y^2 \rangle$ is difference between flux density of linearly polarized beams of light. One is polarized in the x-axis and the second one is polarized in the y-axis. These axes are usually selected to be parallel to horizontal and vertical directions, respectively.
- $S_2 = \langle 2A_x A_y \cos\delta \rangle$ is difference between flux density of linearly polarized beams of light. However, in this case the axes are usually selected to by parallel to diagonal and anti-diagonal directions. It means that the axis is rotated by 45° to the x-axis for the case of diagonal polarization, and by 135° for the case of anti-diagonal polarization.
- $S_3 = \langle 2A_x A_y \sin\delta \rangle$ is difference between flux density of circularly polarized beams of light. One has right-handed circular polarization and the second one has left-handed circular polarization.

These Stokes parameters, as we can see from their definitions, are related with the polarization ellipse (see Equation (14)). Therefore we can rewrite them in the terms of the ellipse parameters

$$\begin{aligned} S_1 &= S_0 \cos(2\varphi)\cos(2\theta), \\ S_2 &= S_0 \cos(2\varphi)\sin(2\theta), \\ S_3 &= S_0 \sin(2\varphi), \end{aligned} \tag{15}$$

where 2φ and 2θ are the spherical coordinates of the three-dimensional vector of Cartesian coordinates (S_1, S_2, S_3). Usually, the total intensity is normalized and $S_0 = 1$. By using the Stokes parameters, we can calculate the degree of polarization DOP

$$DOP = \frac{\sqrt{S_1^2 + S_2^2 + S_3^2}}{S_0}. \tag{16}$$

The light is said to be polarized if $DOP = 1$, unpolarized if $DOP = 0$ and partially polarized if $0 < DOP < 1$.

Stokes parameters can be represented as 4-vectors for various polarization states. Particular 4-vectors are listed in Table 5, where we denote for simplicity the individual polarization states as **H** (resp. **V**) for linear horizontal (resp. linear vertical) polarization, **D** (resp. **A**) for linear diagonal (resp. linear anti-diagonal), and **R** (resp. **L**) for right-handed circular (resp. left-handed circular) polarization.

Table 5: Stokes and Jones vectors for various polarization states

Polarization	H	V	D	A	R	L
Stokes vectors $\begin{bmatrix} S_0 \\ S_1 \\ S_2 \\ S_3 \end{bmatrix}$	$\begin{bmatrix} 1 \\ 1 \\ 0 \\ 0 \end{bmatrix}$	$\begin{bmatrix} 1 \\ -1 \\ 0 \\ 0 \end{bmatrix}$	$\begin{bmatrix} 1 \\ 0 \\ 1 \\ 0 \end{bmatrix}$	$\begin{bmatrix} 1 \\ 0 \\ -1 \\ 0 \end{bmatrix}$	$\begin{bmatrix} 1 \\ 0 \\ 0 \\ 1 \end{bmatrix}$	$\begin{bmatrix} 1 \\ 0 \\ 0 \\ -1 \end{bmatrix}$
Jones vectors	$\begin{bmatrix} 1 \\ 0 \end{bmatrix}$	$\begin{bmatrix} 0 \\ 1 \end{bmatrix}$	$\frac{1}{\sqrt{2}}\begin{bmatrix} 1 \\ 1 \end{bmatrix}$	$\frac{1}{\sqrt{2}}\begin{bmatrix} 1 \\ -1 \end{bmatrix}$	$\frac{1}{\sqrt{2}}\begin{bmatrix} 1 \\ i \end{bmatrix}$	$\frac{1}{\sqrt{2}}\begin{bmatrix} 1 \\ -i \end{bmatrix}$

Stokes vectors can be represented by points in and on a Poincaré sphere, which is plotted in Figure 19. The sphere has the antipodal points corresponding to a pair of mutually orthogonal state vectors. Points of linear polarization lie on the equator of the sphere. Points of circular polarization lie on the poles. Right-handed polarization is on the upper half of the sphere surface and the left-handed is on the lower half [18].

Polarized light can be also represented by Jones vectors. There are defined by less parameters than Stokes vectors, but they do not describe the unpolarized or partially polarized light [18]. Polarized light is represented by points on Poincaré sphere in comparison with partially polarized or unpolarized light, which are represented by points lying inside the sphere. Jones vectors are listed in Table 5.

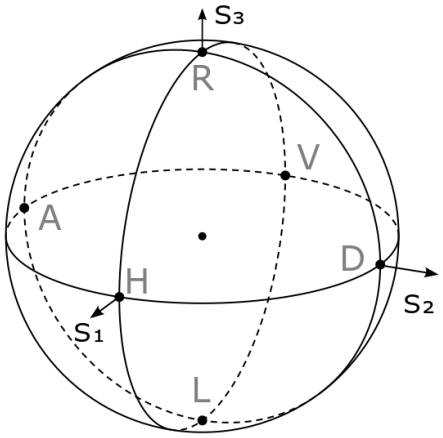

Figure 19: Poincaré sphere.

6.3 Quarter- and half-wave plate calibration

If the polarization state of light is unknown, we can determine it by its projection onto the basis states. Let us consider the mutually unbiased bases H/V, D/A, and R/L, the

probability p of the projected state $|\psi\rangle$ onto some particular basis state is

$$p = \langle\psi|\rho|\psi\rangle, \tag{17}$$

where $|\psi\rangle$ = H, V, D, A, R, L and ρ is the density matrix of the unknown state. This is called the polarization analysis. Particular projections onto basis states are usually done by half-wave (HWP) and quarter-wave plates (QWP). If we want to determine the angles of rotation of HWP and QWP for polarization analysis, we must first calibrate the plates. The purpose of calibration is to determine the angle of rotation of the mount vs angle of rotation of the optics. By calibration we can determine the optic axis of both plates. It can be done by using two linear polarizers as is plotted in Figure 20. Figure 20 (a) shows that for plates calibration at 1550 nm two calcites were used, and Figure 20 (b) shows that for plates calibration at 810 nm was used a pair of PBS. One polarizer serves for the polarization state preparation and the second one serves for its analysis. A single plate (HWP or QWP) is placed between these two polarizers. Then the polarized light passes through the wave plate rotated by an angle γ, where $\gamma \in \langle 0°, 360° \rangle$ and further the polarized light is analyzed. The optic axis can be found by Malus law [19]

$$I = I_0 \cos^2(\gamma - \gamma_c), \tag{18}$$

where I is detected intensity, I_0 is the incident intensity, γ is the angle of plate rotation, and γ_c is the calibration angle.

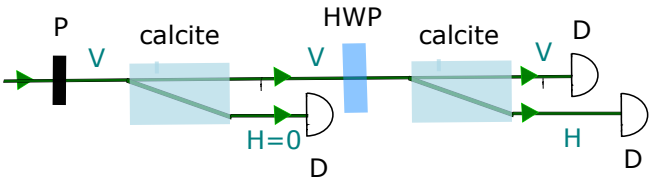

(a) Calibration of plates at 1550 nm.

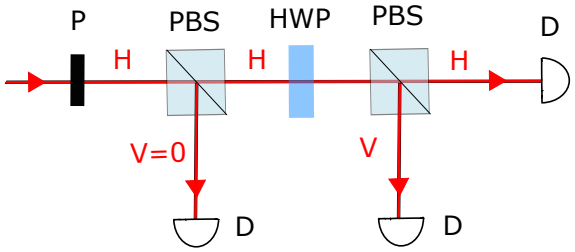

(b) Calibration of plates at 810 nm.

Figure 20: Calibration of wave plates. (a) Calibration at 1550 nm using two calcites. (b) Calibration at 810 nm using a pair of PBS.

Optic axis is defined as a direction, in which the transmitted light suffers no birefringence and if it propagates along the optic axis, it does not change its polarization state. Optic axis of HWP (QWP) is given by one of the maxima of Equation (18).

Once we determine the HWP and QWP optic axes, we can calculate the angles, under which we can rotate the plate to project the unknown polarization state onto one of the basis polarization states. The calculation can be done by using Jones vectors and matrices [20]. The matrix of the wave plate is given by

$$WP = \begin{bmatrix} \exp\left(i\frac{\Gamma}{2}\right) & 0 \\ 0 & \exp\left(-i\frac{\Gamma}{2}\right) \end{bmatrix}, \tag{19}$$

where Γ is retardation. If $\Gamma = \pi$, then we get the matrix of HWP and if $\gamma = \pi/2$, then we get the matrix of QWP. If the wave plate is rotated by some angle γ, the output vector describing the polarization state is multiplied by the rotation matrix $R(\gamma)$

$$R(\gamma) = \begin{bmatrix} \cos\gamma & -\sin\gamma \\ \sin\gamma & \cos\gamma \end{bmatrix}. \tag{20}$$

6.3.1 Wave plate calibration measurement

Optic axis of each plate was found by measuring the output power always, when the plate was rotated by 5° in range $[0°, 360°]$. Intensity dependences of HWP and QWP for both wavelengths on the angle are plotted in Figure 21. Measured data are fitted by function corresponding to Malus law in Equation (18)

$$f(x) = a + b\cos^2(cx + d), \tag{21}$$

where a, b, c, and d are constants given by individual fits.

The rotation angle of the plate, which corresponds to the propagation of the input light along the optic axis of the plate, can be found by determining the maxima of the function in Equation (21). For the case of HWP, the angle was chosen as the first maximum, and in case of QWP the angle was chosen as the third maximum, because there the individual fits best fit the measured data. After determination of optic axis of all four wave plates, projection angles onto basis polarization states were found by using Jones notation. Then calibration measurements using the calculated angles were made. In each measurement, the input light were polarized into H state by polarizer. Subsequently, the plate was rotated to an angle that corresponded to projection onto one of the basis polarization states (H, V, D, A, R, L). The polarized light then passed through another polarizer to the detector, where the signal was detected. It was done for all four plates. The resulting polarization states always corresponded to the setting of the individual plates with $DOP = 1$.

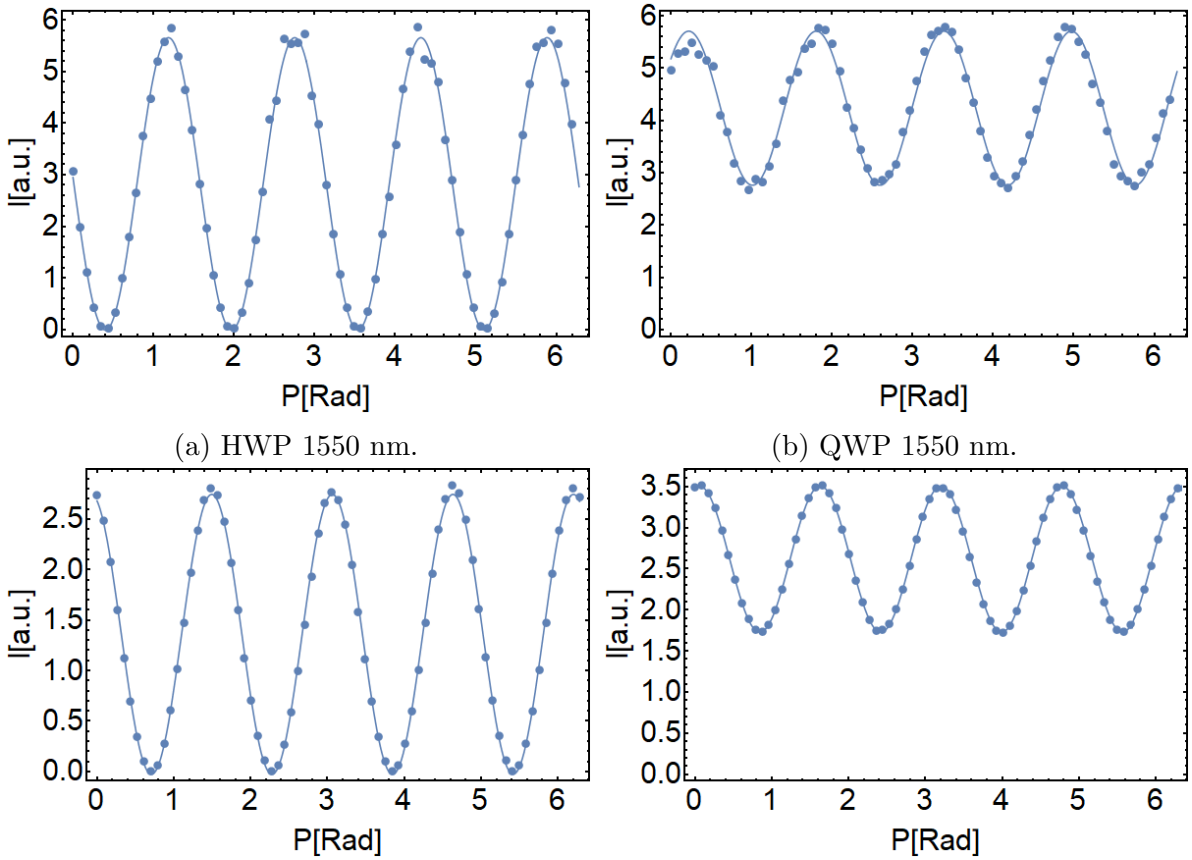

(a) HWP 1550 nm.

(b) QWP 1550 nm.

(c) HWP 810 nm

(d) QWP 810 nm.

Figure 21: Measured intensity depenence on angle. Measured data are fitted by function corresponding to Malus law.

6.4 Telecommunication fiber link

The telecommunication fiber link should transfer two beams of light at different wavelengths. The one at 1550 nm should serve to stabilize the link and the second one at 810 nm should transfer information over the fiber link. Two fiber coupled laser diodes - QFLD-810-10S-SM (λ = 810nm) and FOSS-01-3S-9/125-1550-S-1-ISOL (λ = 1550 nm), were connected by optical adapter to polarization controller, which sets the desired polarization states of each LD. The light at both wavelengths were coupled out into free space. Wavelength of 1550 nm were coupled out by optic collimator C220 TME-B with a focal length f = 11 mm made by Thorlabs and other optic collimators used in this experiment were 60FC-0-A11-02 (SN:000677) with a focal length f = 11 mm by Schäfter + Kirchhoff. Using two mirrors (BB1-E04 for λ = 1550 nm and BB1-E03 for λ = 810 nm), the beam of light was directed to a dichroic mirror (wave separator made by Altechna, 1-0S-2-0254-5- (4N45), R = 800 nm, T = 1550 nm). This type of mirror transmits the beam of light at 1550 nm and reflects the beam of light at 810 nm in 90°. Both beams were directed to enter the dichroic

mirror under a certain angle, so they became collinear. The beams then went through the polarizer together into the optic collimator, where they were coupled in SMF 28e$^+$. This single mode fiber has the same type as FUT. We placed it here mainly for manipulation with FUT without changing the coupling efficiencies. The fibers were placed at the both sides of FUT. The one at the output end of FUT was a part of polarization controller for 1550 nm and led to the optic collimator. The beams of light at both wavelengths then continued in free space to the dichroic mirror of the same type, as was the first one. The mirror caused a split of these two different wavelengths. 1550 nm continued in the same direction and 810 nm was reflected in 90°. Then at both wavelengths, the polarization analysis was applied.

The beam at 1550 nm went through the polarization analysis, which consisted of HWP (ZO-L/2-1550 by EKSMA) and QWP (ZO-L/4-1550 by EKSMA) placed in rotation motorized holders, into a calcite prism. It acts as beam displacer and splits H and V polarization. Due to birefringence, V polarization passed through this beam displacer in unchanged direction, but H polarization direction was deflected. Finally, H polarized light reached the detector PDA20CS-EC and V polarized light reached the detector PDA 10CS-EC. In front of both detectors, we placed cut-off filters BG3 AR780 by Eksma Optics, which filtered out wavelengths less than 700 nm.

The beam at 810 nm went through the polarization analysis, which constisted of HWP (ZO-L/2-0800 by EKSMA) and QWP (ZO-L/4-0800 by EKSMA), continued into a filter FBH810-10 by Thorlabs with central wavelength is CWL= 810$\pm$2 nm and full width at half maximum FWHM=10$\pm$2nm and then reached PBS. It splits H and V polarization. But H polarization passed through PBS without a change of its direction and V polarization was reflected in 90°. H and V polarized beams of light were then coupled in SMF 780-HP to filter out created higher spatial modes. Finally, 780-HP fibers were connected to detectors PDA 36A-EC. Schema of our telecommunication optical fiber link is plotted in Figure 22.

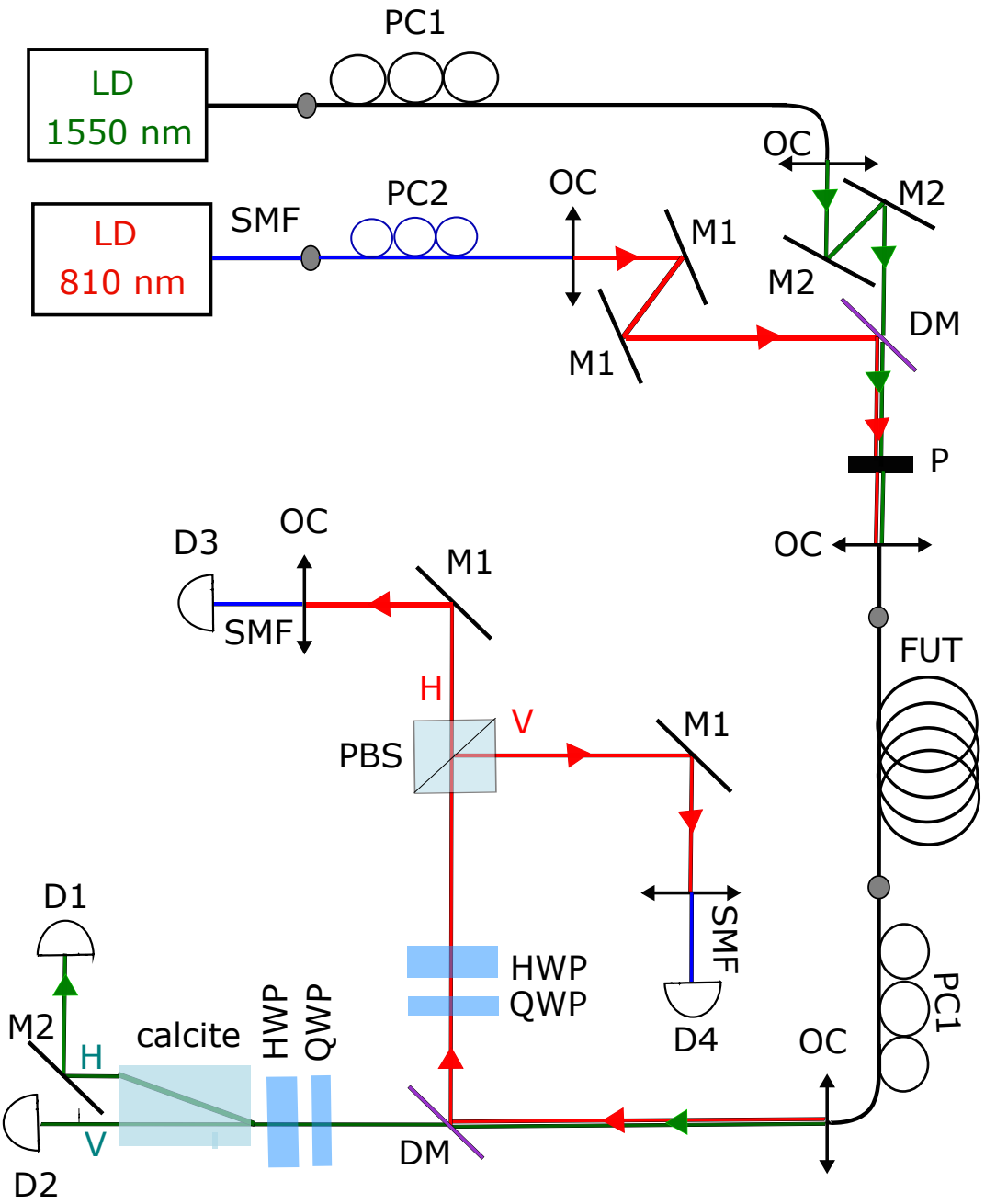

Figure 22: Telecommunication fiber link connecting two different wavelengths - 810 nm and 1550 nm. LD - laser diode, SMF - single mode fiber, small round gray point - optical adapter, PC1 (PC2) - polarization controller for 1550 nm (810 nm), OC - optic collimator, M1 (M2) - mirror for 1550 nm (810 nm), DM - dichroic mirror (wave separator), P - polarizer, HWP - half wave plate, QWP - quarter wave plate, PBS - polarization beam splitter, D1, D2 - detectors at 1550 nm, and D3, D4 - detectors at 810 nm.

6.5 Calibration measurement

The calibration measurement was done in three different ways further described as I), II), and III). Before a long-term measurement of polarization drift, we first performed the calibration measurements described in I) and II) and found out how fast the polarization changed over time, which is part of the measurement described in III).

I) Projections of individual basis polarization states by QWP and HWP were measured without FUT. Just two short optical fibers of the same type as the FUT were connected together. The beam of light was horizontally polarized by an added polarizer placed in front of the second dichroic mirror. The shema is plotted in Figure 23. All 6 projections were made to verify, if our calculated projection angles of the individual plate are correct, i.e. if our input state is projected onto the output state of wanted polarization.

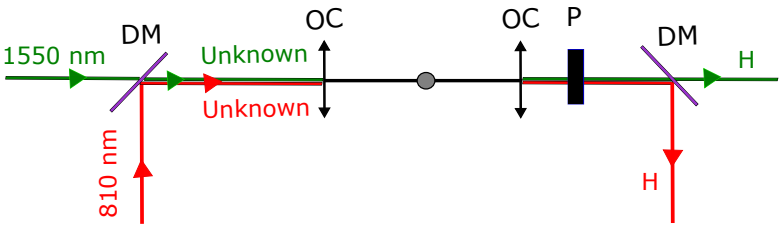

Figure 23: Calibration measurement using polarizer and two short (1 m) fibers of the same type as the FUT. Polarization state of both beams at different wavelengths entering the fibers is unknown. After the beams pass through the fibers, they are subsequently horizontally polarized by the polarizer. DM - dichroic mirror, OC - optic collimator, P - polarizer, and small gray round point - optical adapter.

II) Then the polarizer was moved behind the first dichroic mirror to set the polarization of light, which is coupled in two short optical fibers. Schema is plotted in Figure 24. The input polarization state of light set by polarizer was changed as light propagated over the fibers. Hence, the polarization state of light passed through the fibers was set by a polarization controller (PC), but only for 1550 nm. Wavelength of 810 nm had unknown output polarization state.

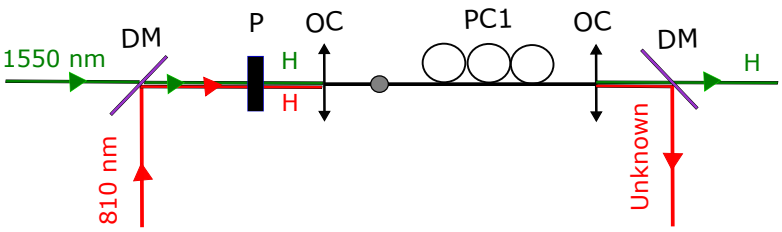

Figure 24: Calibration measurement usning PC and two short (1 m) optical fibers of the same type as the FUT. Polarization states set by polarizer at the beginning are changed due to propagation in the FUT. Output polarization state of light at 1550 nm is set by PC to H polarization and 810 nm has unknown polarization state. DM - dichroic mirror, OC - optic collimator, P - polarizer, PC1 - polarization controllers for 1550 nm, and small gray round point - optical adapter.

III) Finally, we placed FUT between two short optical fibers in the setup. The length of FUT was 4 km (made by connection of 1 km and 3 km long FUT). We repeated both measurement described in I) and II).

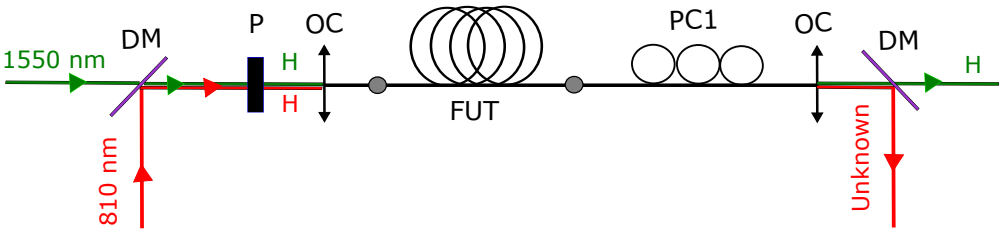

Figure 25: Calibration measurement with 4 km long FUT placed between two short optical fibers for the measurement described in II). DM - dichroic mirror, OC - optic collimator, P - polarizer, PC1 - polarization controllers for 1550 nm, and small gray round point - optical adapter.

The desired polarization states with $DOP \approx 1$ were measured in I) and II). The calibration measurement in III) was done only using 3-base projection H/V, D/A, and R/L. Due to it, the coupling and detection efficiencies had to be known. It meant that the detectors had to be calibrated to each other - mainly for 1550 nm, because they were not of the same type. After that, Stokes vectors were calculated from the measured data. They are plotted in the Poincaré sphere in Figure 26. There we can see the change of polarization state in 4 km long FUT depending on time for both type of calibrations. The output polarization states with $DOP \in (0.8, 1)$ slowly vary over time. However, this variation in polarization may also be given by a variation of fiber coupling efficiency due to laboratory conditions. Considering this fact and the slowly varying polarization over time, the following polarization analysis was done by projection onto all six basis polarization states.

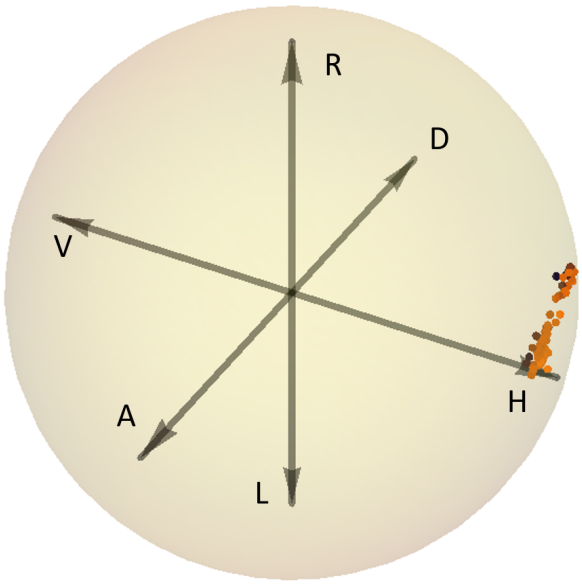

(a) Measurement described in I) at 1550 nm.

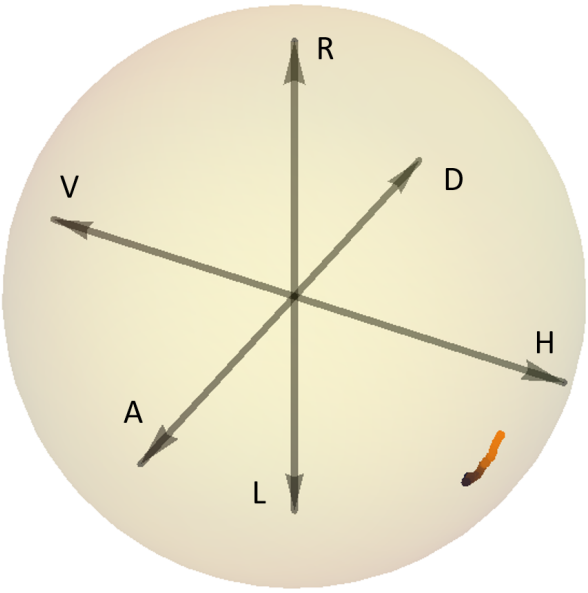

(b) Measurement described in I) at 810 nm.

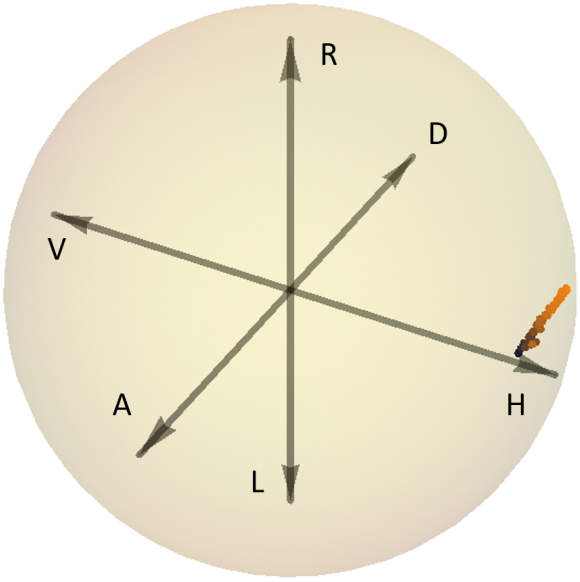

(c) Measurement described in II) at 1550 nm.

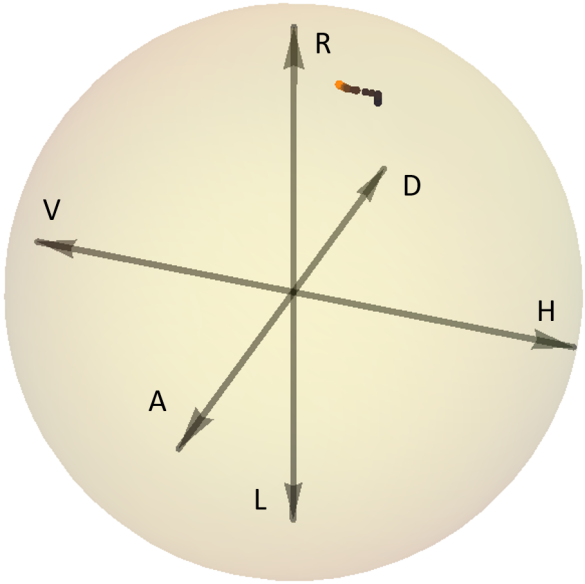

(d) Measurement described in II) at 810 nm.

Figure 26: Calibration of HWP and QWP. There we can see the change of polarization state within 7 hours. The color is chosen in shades of orange, from the lightest to the darkest color, so that the change in polarization state is clearly visible. (a) ((b)) Polarization state of light set on H polarization using polarizer at 1550 nm (at 810 nm). (c) Polarization state of light set on H polarization using PC at 1550 nm with undefined polarization state at 810 nm, which is plotted in (d).

6.5.1 Polarization analysis measurement

Polarization analysis was measured in the similar way as the calibration. The two main differences are the duration of the measurement and the choice of the number of polarization states projections. As was mentioned above, the analysis is measured using six polarization states projections. The reason is the possibility to omit the fiber coupling efficiencies, which can cause an error in the polarization state reconstruction. We used our built telecommunication fiber link to measure how polarization of light varies over time. The scheme is in Figure 22.

The polarization analysis measurement was done as is described in II) but with added 4 km long FUT. A polarizer was used in this experiment to set the polarization state of two beams of light at different wavelengths, which were coupled into FUT. Polarization of light passed through FUT was set by a polarization controller (PC), but only for a case of 1550 nm. 810 nm had undefined polarization state. Then output beams continued through the free space into the dichroic mirror, where they were separated and each went into its own polarization analysis made of HWP and QWP. The setup is plotted in Figure 25. The polarization analysis was measured for 60 hours and the results are plotted in Figure 27. Figures 27(a) and (b) show the reconstruction of polarization states only from one detector at 1550 nm and at 810 nm, respectively. The measured values are displayed in different shades of orange to see the changes in the polarization state.

The next two Figures 27 (c) and (d) show the reconstruction of the polarization state using both detectors, by which the polarization analysis for given wavelengths was measured. Figure 27(c) is slightly rotated in comparison with (a) to see the directions of polarization changes. The evolution of the polarization state over time is very similar for both detectors.

We can also notice that the degree of polarization is significantly worse than in case of calibration (when it was almost equal to 1). One of the possible reasons is that coupling efficiency of detectors could change during the rotation of plates. However, this is only the subject of speculation and the measurement will be repeated. At the moment, we can say that our polarization analysis indicates that the polarization state is evolving over time, but its change is not very large.

All measurements were made when the fiber was in a spool. Another object of investigation will be to determine how the deployed fiber behaves if we change its surrounding conditions.

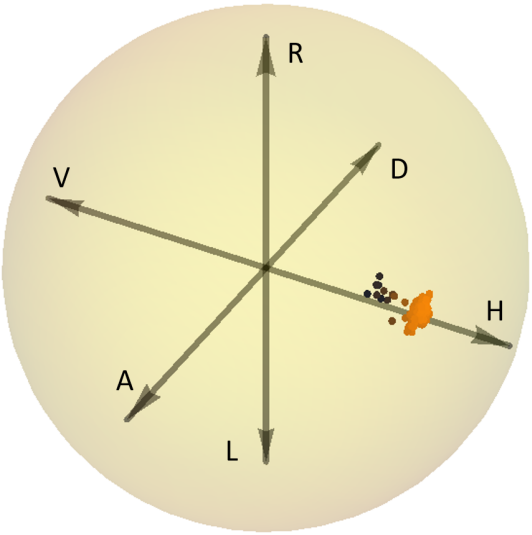

(a) Measurement of polarization state at 1550 nm made by D1.

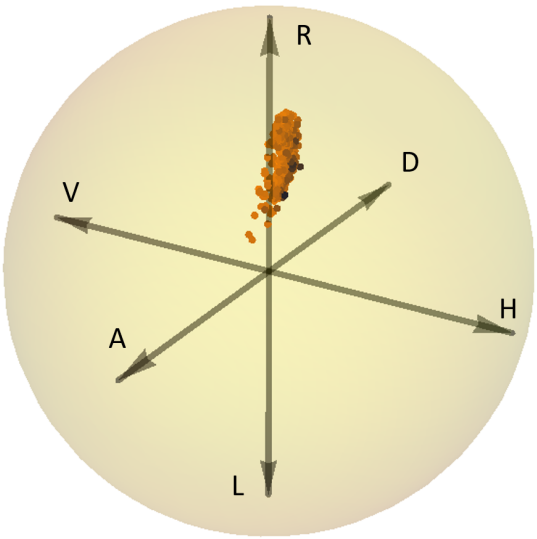

(b) Measurement of polarization state at 810 nm made by D3

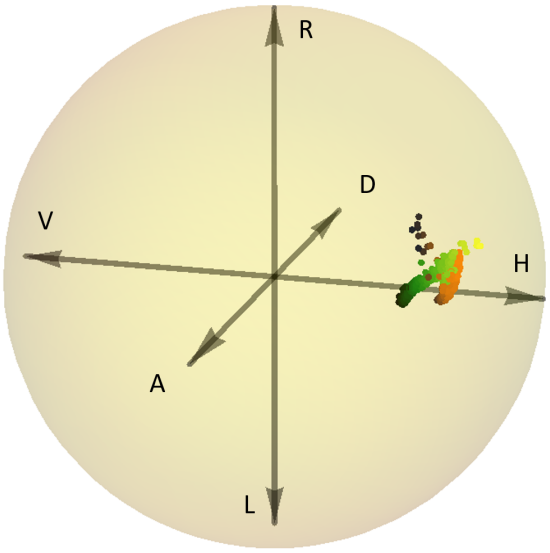

(c) Measurement of polarization state at 1550 nm made by 2 detectors (D1 and D2).

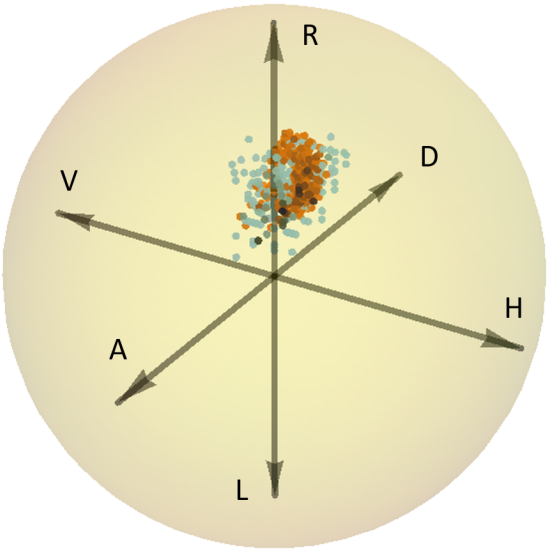

(d) Measurement of polarization state at 810 nm made by 2 detectors (D3 and D4).

Figure 27: Measurement of polarization states of two beams at different wavelengths - 1550 nm and 810 nm. All six projections onto basis polarization states were use to reconstruct the output polarization states and their evolution over time. (a) and (b) show reconstructed polarization states only from one detector: D1 in case of 1550 nm and D3 in case of 810 nm. (c) and (d) show the same polarization state reconstructed from both detectors D1, D2 (D3, D4 in case of 810 nm). Data from different detectors are distinguished by different colors - orange belongs to the first detector D1 (or D3), green belongs to the second one D2 and blue belongs to D4. These colors are in different shades from the darkest (start of the measurement) to the lightest (end) to see polarization changes over time.

7 Design of telecommunication fiber stabilization

A polarized beam of light might have a different polarization state after propagation over a long telecommunication optical fiber. The reason is mainly a birefringence induce by the unavoidable stress or by the fiber asymmetry. If we want to have the same polarization state as the input one, the process of stabilization is necessary. Basically, polarization state stabilization is a matter of automatic control, which means the implementation of a feedback system, i.e. a polarization controller, to invert the adverse effect of the fiber channel.

Stabilization of polarization state is particularly important for quantum cryptography based on the polarization degree of freedom. In fiber-based QKD systems, it is necessary to obtain accurate polarization decoding. In the presence of unpredictable polarization transformation, receiver needs polarization feedback control to recover the initial polarization state [21].

In our case, we have a telecommunication fiber link, which serves to transfer light at two different wavelengths. The one at 810 nm should transfer information over the link. The other one at 1550 nm can be used for the polarization stabilization of the link. In the previous section, the polarization analysis at both wavelengths was performed. We noticed that our measured polarization state slowly varied over time, hence the stabilization does not have to be too fast.

The active polarization stabilization is more complicated than the common single-parameter stabilization feedback loop. A polarization state is represented by the Stokes vector or two spherical angular coordinates of the Poincaré sphere. In case of time evolution of polarization state in fibers, both coordinates may drift monotonically and also fluctuate randomly. Their deviations from the corresponding setpoints have to be evaluated repeatedly and fed to a polarization controller correcting the polarization state, as is plotted in Figure 28.

The optical component compensating for changes in polarization state could be for example a component with rotating birefringent axes or just a common retarder, but the reset procedure is required in this case. The stabilization may be also done by electronic polarization controllers (EPC) consisting of piezoelectric actuators, which are used to stress the fibers along different directions. This induces the desired birefringence in the fiber to adjust the polarization state.

The measurement is performed at 1550 nm, however, the polarization state should be locked at 810 nm. The active feedback loop has to take into account different action of the FUT and the polarization controllers as well at these wavelengths. The polarization state stabilization will be subject of the future work.

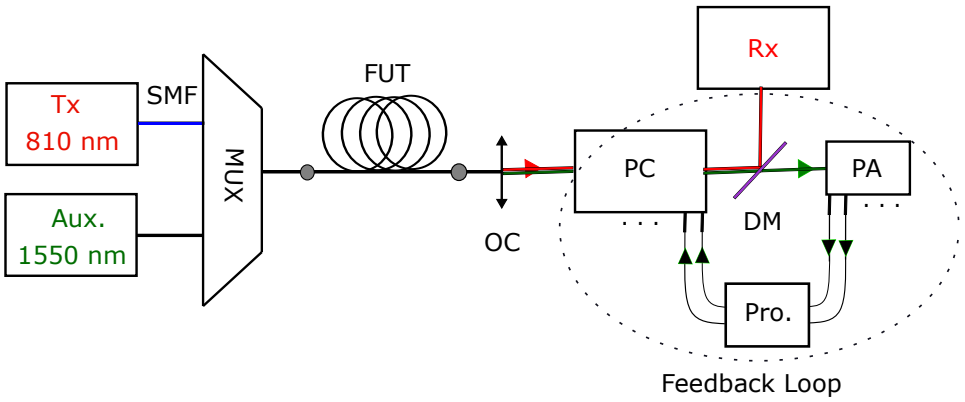

Figure 28: Design of telecommunication fiber stabilization. Tx - transmitter, Aux. - auxiliary signal, SMF - single mode fiber, MUX - multiplexer, OC - optic colimator, PC - polarization controller, DM - dichroic mirror, Rx - receiver, PA - polarization analysis, and Pro. - processing.

8 Conclusion and discussion

The purpose of this work was to build, analyze and characterize an optical fiber link working at two different wavelengths: 810 nm and 1550 nm. All measurements were done for FUT complying to G. 652D, because this thesis dealt with a possibility of information transfer at 810 nm over telecommunication fiber link. The investigated phenomena, which can limit the communication in fibers, were mainly losses depending on FUT length and also on wavelength, modal dispersion, channel fading in fibers, and changes of polarization states in FUT over time. At the end of this work it is also suggested a possible correction of the polarization instabilities of our telecommunication optical fiber link.

In telecommunication fibers, the wavelength of 810 nm has higher losses in comparison with 1550 nm. We have determined the losses at both wavelengths by using different FUT lengths. In case of 1550 nm, the attenuation coefficient describing losses in the FUT was (0.19 $\pm$ 0.04) dB/km and in case of 810 nm, the attenuation coefficient was (2.35 $\pm$ 0.02) dB/km. Even though the losses at 810 nm are several times higher than for 1550 nm, it is still possible to transfer information at 810 nm over telecommunication fiber link within several kilometers.

Another limiting effect in the optical telecommunication fiber link is modal dispersion. The signal at 810 nm shows multi-mode behavior. We have determined that the FUT at 810 nm supports just two spatial modes - LP_{01} and LP_{11} - and with increasing length of the FUT the distance between these spatial modes also increases. Time delay between individual spatial modes is a linear function of FUT length. The measured average delay per 1 km was (2.1 $\pm$ 0.2) ns. We also found out that by connecting 6.5 cm long single mode fiber 780-HP to the FUT, the higher modes at 810 nm are filtered out and the transmittance of 1550 nm is 50%.

Effects described above can be also analyzed by optical time domain reflectometry

(OTDR). But in this work, the method was used to determine the effective refractive index of our FUT at 810 nm. In the case of 1 km long FUT, the effective refractive index was 1.48 ± 0.03 and in the case of 3 km long FUT, the effective refractive index was 1.50 ± 0.01.

After determining the effect of dispersion and the amount of losses at 810 nm in the FUT, we made several longer measurements to determine behavior of transmittance in time. Measurements of the effect known as channel fading were made within 32 hours and they were evaluated by Allan deviation and by using histograms. We measured this effect for 1 km, 4 km, and 10 km long FUT. Fluctuations in the FUT were found to be increasing from 0.008% in the case of 1 km long telecommunication fiber to 0.05% in the case of 10 km long telecommunication fiber. The transmittance fluctuations were not caused only by the measuring apparatus, because the measurement was made also for the case without FUT. In this case, fluctuations were not as large as in the cases with connected FUT. However, individual measurements of transmittance fluctuations in the FUT were made under different laboratory conditions. This is probably the main cause of the different shapes of the histograms. However, fiber channel fading is not explored in the literature and will be studied in the future work.

One of the main steps in optical fiber link characterization is polarization analysis. It contains measuring of changes of polarization states passed through FUT over time. Initially, we started with calibration measurements, which included determining of the optic axes of HWP and QWP, by which the polarization analysis was performed. We also calculated all projection angles, which projected our output state into one of the basis polarization states. Then several calibration measurements with and without the 4 km long FUT was made. We use 3-base projection and 6 states projection of polarization. We also did measurement lasting 7 hours. In all these measurements we get the desired polarization state with $DOP \in \langle 0.8, 1 \rangle$. Furthermore, we determined that the polarization state vary slowly over time. Then we made polarization analysis lasting 60 hours using 6 projections of polarization states. Unfortunately, DOP values were less than in the case of calibration measurements. However, the measurement will be redone. We have found that polarization states change very slowly over time. As a result, the feedback loop for polarization stabilization may not be too fast.

Finally we suggested correction of polarization instabilities. The main idea is to use the wavelength at 1550 nm to create a feedback loop to stabilize the entire optical fiber link. The next goal realize the stabilization feedback loop and verify polarization encoded communication at 810 nm over the telecommunication fiber.

References

[1] Mohammad-Ali Khalighi, Murat Uysal: *Survey on Free Space Optical Communication: A Communication Theory Perspective*. IEEE Communications Surveys & Tutorials 16(8):2231-2258. November 2014.

[2] Hua.Lei Yin, Teng-Yun Chen, Zong Weng YU, *etal*: *Measurement-device-independent quantum key distribution over a 404 km optical fiber*. DOI: 10. 1103/PhysRevLett. 117. 190501.

[3] P. D. Townsend: *Experimental investigation of the performance limits to first telecommunication- window quantum cryptohrapgy systems*. IEEE PHOTONICS TECHNOLOGY LETTERS, VOL. 10, NO. 7, JULY 1998.

[4] C. Holloway, E. Mayer-Scott, Ch. Erven, and T. Jennewein: *Quantum entanglement distribution with 810 nm photons through active telecommunication fibers*. Optics Express, 20597 (2011).

[5] E. Mayer-Scott, H.Hübel, A. Fedrizzi, C. Erven, G. Weiths, and T. Jennewein: *Quantum entanglement distribution with 810 nm photons through telecom fibers*. Applied physics letters, **97**, 031117 (2010).

[6] G. P. Berman, A. A. Chumak, and V.N. Gorshkov: *Beam Wandering in the Atmosphere:The Effect of Partial Coherence*.Physical Review E 76(5 Pt 2):056606 . December 2007.

[7] D. W. Allan: *Statistics of atomic frequency standards*. Proceedings of the IEE. vol. 54, NO.2. February 1966.

[8] G. P. Agrawal: *Fiber-Optics Communication Systems*. 4th Edition. John Wiley & Sons, Inc., Publication, 2010. Rochester, New York.

[9] Saleh, B.E.A., Teich, M.C.: *Fundamentals of Photonics*. 2nd Edition. John Wiley & Sons, Inc, 2007. New York. ISBN:978-0471358329.

[10] http://what-when-how.com/fiber-optics/optical-fiber-communication-technology-and-system-overview-part-1/, (25. 10. 2018)

[11] $http://www.fiberoptics4sale.com$. 15. 12. 2018

[12] John M. Senior: *Optical Fiber Communications*. 3rd Edition. Pearson/Prentice Hall, 2009. UK. ISBN: 978-0-13-032681-2.

[13] D.Gloge: *Weakly guiding fibers*. 2252 APPLIED OPTICS / Vol. 10, No. 10 / October 1971

[14] $https://www.rp-photonics.com/lp_modes.html$. (20. 4. 2019)

[15] Jerzy Siuzdak: *Influence of modal filtering on the bandwidth of multimode optical fibers.* Instytut Telekomunikacji Politechniki Warszawskiej.Warszawa, Poland.

[16] Jimmy Gagnon: Inderstanding OTDRs. Optical Business Unit, Application note 194; EXFO [4]. GN Nettest, Part #33881 Rev. February 2000.

[17] Y. Yeh: *Photonics - Optical electronics in modern communications.* Sixth edition. Oxford University Press, 2007, New York.

[18] R. D. Guenther: *Modern Optics.* John Wiley & Sons, Inc, 1980, New York. ISBN: 0-471-60538-7.

[19] Dipak Basu: *Pure and applied physics.* CRS Press LLC, 2001, Washington D.C. ISBN: 0-8493-2890-X.

[20] J. Peatross, M Ware: *Physics of Light and Optics.* Brigham Young University. 2015. ISBN: 978-312-92927-2.

[21] Jie Chen, Guang WU, Yao Li, E. WU, and Heping Zeng: *Active polarization stabilization in optical fibers suitable for quantum key distribution.* 24 December 2007 / Vol. 15, No. 26 / OPTICS EXPRESS 17928. OSA 2007.

Appendices

A Photo of the experiment

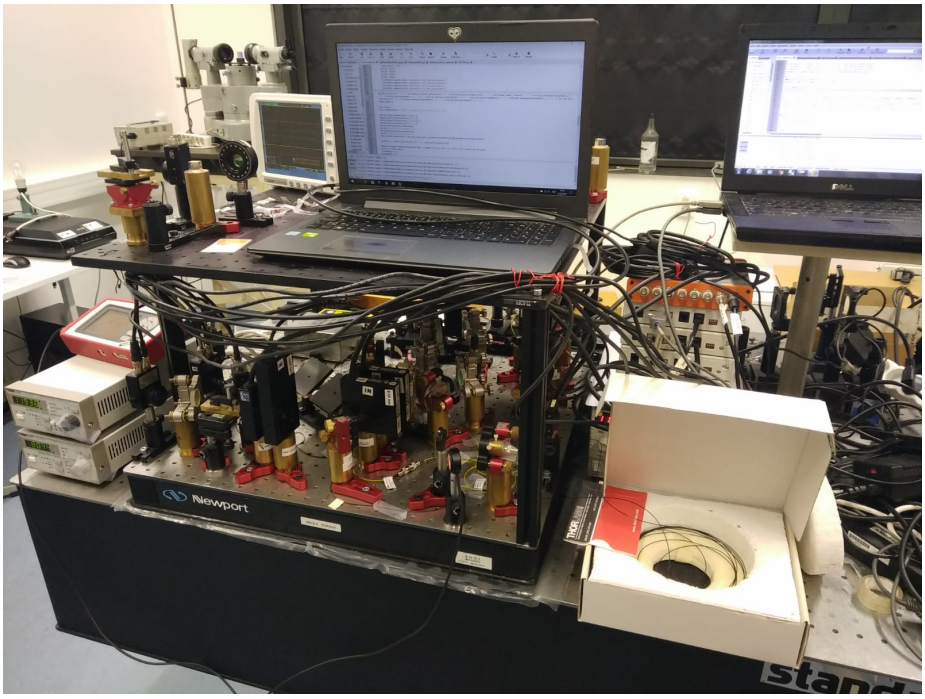

Figure 29: Photo of the experimental setup. Complete telecommunication optical fiber link. The laser diodes for two different wavelengths at 1550 nm and 810 nm are situated behind detectors, which representing the fiber link end. In the middle part of our link, we can see polarization analysis consisted of half- and quarter-wave plates. On the right side, there is the fiber under test in spool.

B List of Abbreviations

ADC	Analog-to-digital converter	LD	Laser diode
BS	Beam splitter	LP	Linear polarized
DOP	Degree of polarization	PC	Polarization controller
CWL	Central wavelength	SMF	Single mode fiber
FUT	Fiber under test	SN	Serial number
FWHM	Full width at half maximum	QKD	Quantum key distribution
HWP	Half-wave plate	QWP	Quarter-wave plate
OTDR	Optical time domain reflectometry		